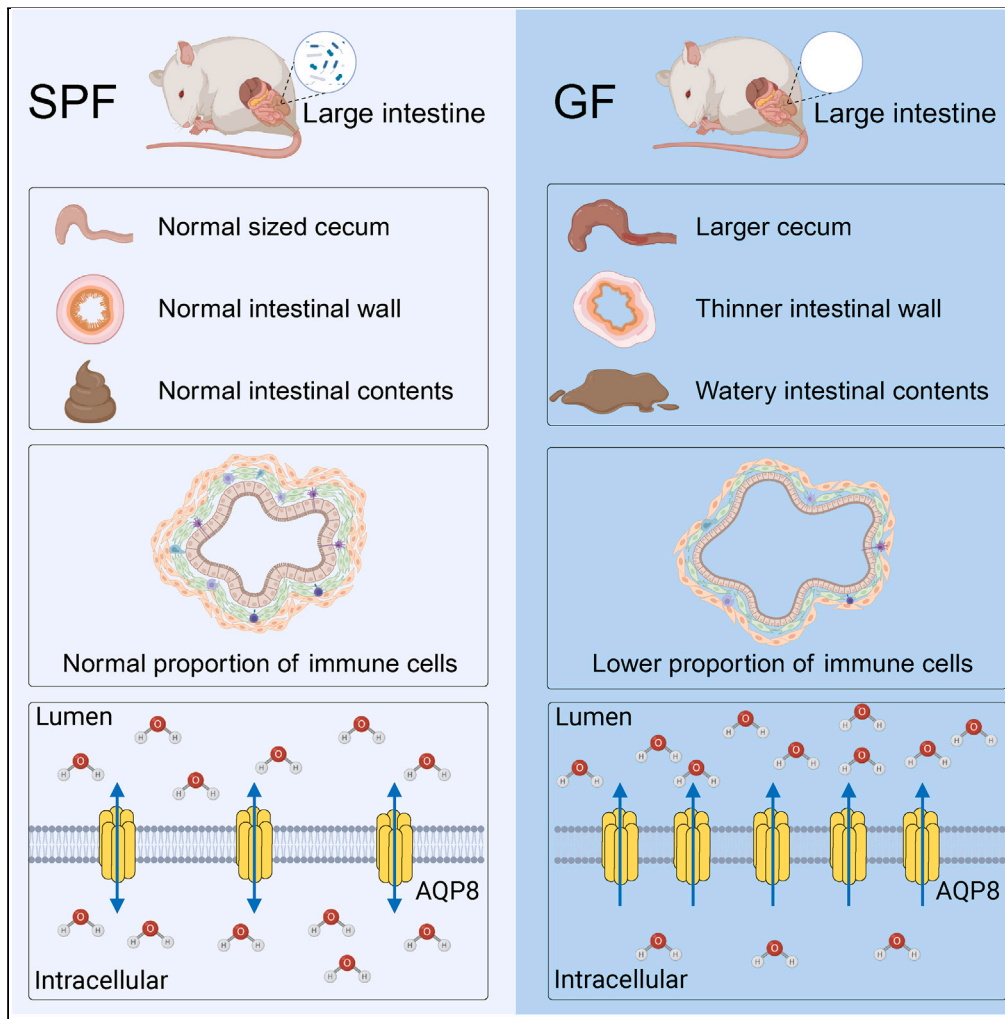


Article

# Effects of flora deficiency on the structure and function of the large intestine



Tailiang Chai, Juan Shen, Yifei Sheng, ..., Aibo Gao, Hong Wei, Xiaodong Fang

weihong63528@163.com (H.W.)  
fangxd@bgi.com (X.F.)

**Highlights**

Spatiotemporal transcriptome atlas of the large intestine of GF and SPF mice

Increased AQP8 in enterocytes leads to more water secretion into the intestinal lumen

Reduced extracellular matrix building function relates to thinning of the GF gut wall

GF large intestine has increased nutrient absorption and decreased immune function

Chai et al., iScience 27, 108941  
February 16, 2024 © 2024 The Authors.  
<https://doi.org/10.1016/j.isci.2024.108941>



## Article

## Effects of flora deficiency on the structure and function of the large intestine

Tailiang Chai,<sup>1,2</sup> Juan Shen,<sup>2</sup> Yifei Sheng,<sup>1,2</sup> Yufen Huang,<sup>2</sup> Weiming Liang,<sup>2</sup> Zhao Zhang,<sup>1,2</sup> Ruizhen Zhao,<sup>1,2</sup> Haitao Shang,<sup>3</sup> Wei Cheng,<sup>4</sup> Hang Zhang,<sup>4</sup> Xueting Chen,<sup>1,2</sup> Xiang Huang,<sup>1</sup> Yin Zhang,<sup>1,2</sup> Jiazhe Liu,<sup>2</sup> Huanjie Yang,<sup>2</sup> Linying Wang,<sup>2</sup> Shanshan Pan,<sup>5</sup> Yang Chen,<sup>6</sup> Lijuan Han,<sup>7</sup> Qinwei Qiu,<sup>6</sup> Aibo Gao,<sup>8</sup> Hong Wei,<sup>3,\*</sup> and Xiaodong Fang<sup>2,6,9,\*</sup>

## SUMMARY

**The significant anatomical changes in large intestine of germ-free (GF) mice provide excellent material for understanding microbe-host crosstalk. We observed significant differences of GF mice in anatomical and physiological involving in enlarged cecum, thinned mucosal layer and enriched water in cecal content. Furthermore, integration analysis of multi-omics data revealed the associations between the structure of large intestinal mesenchymal cells and the thinning of the mucosal layer. Increased *Aqp8* expression in GF mice may contribute to enhanced water secretion or altered hydrodynamics in the cecum. In addition, the proportion of epithelial cells, nutrient absorption capacity, immune function and the metabolome of cecum contents of large intestine were also significantly altered. Together, this is the first systematic study of the transcriptome and metabolome of the cecum and colon of GF mice, and these findings contribute to our understanding of the intricate interactions between microbes and the large intestine.**

## INTRODUCTION

The intestine is an important digestive and immune organ in mice, playing a key role in nutrient digestion and absorption, immune response, resistance to invasion by intestinal microorganisms, waste removal, hormone regulation and neuromodulation.<sup>1–3</sup> Pathological conditions affecting the intestine may give rise to various ailments, posing a serious health risk.<sup>4–8</sup> A comprehensive understanding of the complex mechanisms underlying gut function is imperative for preserving intestinal health and identifying and treating intestinal disorders. The trillions of symbiotically residing microorganisms on the surface of the intestinal epithelium significantly impact the host's health and susceptibility to diseases, rendering the intestinal microbiota an indispensable "vital organ" and a "second genome" of the body.<sup>9–13</sup>

All organisms inevitably encounter and interact with the microbiota. Both the environmental microbiota and the gut microbiota affect the host in different ways, some of which are manifested as changes in host phenotype and function.<sup>14</sup> And most of the current research has focused on exploring the link between microbiota composition and host disease and health.<sup>15–18</sup> These studies often lack comprehensive and systematic investigations. Our understanding of how the microbiota affects the host remains inadequate, particularly in terms of the effects of the gut microbiota on intestinal cellular composition, function, cellular metabolism, spatial distribution, and intestinal structure. The germ-free (GF) mice, which live in an aseptic environment and lack the influences of the intestinal microbiota, are an important resource for exploring these influences from the perspective of a deficient microbiota.<sup>19</sup> A systematic comparison can provide a comprehensive understanding of how the gut microbiota shapes and influences the structure and function of the host gut, ultimately helping us to understand the importance of gut microbiota-host symbiosis.

The cecum is a sac-like organ, located at the junction of the ileum and proximal colon, that provides storage for fiber-rich plant foods in herbivores, while the large number of co-bacteria in the cecum will contribute to the enzymatic breakdown of plant matter.<sup>20</sup> There are some obvious anatomical and functional changes in the cecum of GF mice relative to specific pathogen-free (SPF) mice, such as a 9 times larger cecum, thinner cecal wall, which provide excellent material for understanding the effect of intestinal microbiota on the host gut.<sup>21,22</sup> The colon

<sup>1</sup>University of the Chinese Academy of Sciences, College of Life Sciences, Beijing, Beijing, China

<sup>2</sup>BGI, Shenzhen, Guangdong, China

<sup>3</sup>Sun Yat-sen University First Affiliated Hospital, Precision Medicine Institute, Guangzhou, Guangdong, China

<sup>4</sup>Huazhong Agricultural University, College of Animal Sciences and Technology, Wuhan, Hubei, China

<sup>5</sup>BGI-Qingdao, Qingdao, Shandong, China

<sup>6</sup>State Key Laboratory of Dampness Syndrome of Chinese Medicine, The Second Affiliated Hospital of Guangzhou University of Chinese Medicine, Guangzhou, Guangdong, China

<sup>7</sup>Department of Scientific Research, Kangmeihuada GeneTech Co., Ltd. (KMHD), Shenzhen, China

<sup>8</sup>Department of Endocrine and Metabolic Diseases, Shanghai Institute of Endocrine and Metabolic Diseases, Ruijin Hospital, Shanghai Jiao Tong University School of Medicine, Shanghai 200025, China

<sup>9</sup>Lead contact

\*Correspondence: [weihong63528@163.com](mailto:weihong63528@163.com) (H.W.), [fangxd@bgi.com](mailto:fangxd@bgi.com) (X.F.)

<https://doi.org/10.1016/j.isci.2024.108941>



is intermediate between the cecum and rectum and is colonized by a large number of microorganisms. The relationship between the microbial composition of the colon and host disease and health is widely appreciated.<sup>23</sup>

This study utilized liquid chromatography-mass spectrometry (LC-MS), single-cell, and spatial transcriptomic techniques to explore the effects of gut microbiota on the structural and functional aspects of the cecum and colon in GF and SPF mice (Figure 1A). To eliminate potential confounders associated with dietary differences, we standardized the diets of both groups of mice to ensure that the observed differences between GF and SPF mice were predominantly due to the lack of gut microbiota. Our findings provide elucidation on the molecular mechanisms responsible for the anatomical changes in the cecum and colon, along with functional alterations across multiple cell types in the large intestine. These results fill significant research gaps within the field of GF mice and provide valuable insights into gut-microbe-gut interactions. For the first time in the field of GF mice, this study applies multi-omics approaches to investigate the large intestine and serves as a critical resource for future research in this area.

## RESULTS

### Anatomical changes in the cecum of GF mice

The GF cecum underwent significant anatomical changes compared to the SPF cecum. We observed an approximately 9-fold increase in the weight of the GF cecum (Figures 1B, 1D, S1A, and S1B). H&E staining showed a significant decrease in the mucosal thickness of the GF cecum (Figure 1C). Anatomical statistics showed that the wall of the GF cecum was approximately one-third thinner (Figure 1E). In addition, we observed an increase in the water content of the GF cecum contents in a semi-liquid state. In conclusion, our anatomical observations suggest that the absence of gut microbiota significantly affects the structure of the cecum.

### Single-cell transcriptome atlas of the GF and SPF mouse cecum

To elucidate the transcriptional response of cecum cells to microbiota, single-cell RNA sequencing (scRNA-seq) was conducted on four cecum samples obtained from identical tissue locations in GF and SPF mice. After removal of substandard cells and adjustment for batch effects while accounting for individual variability, a total of 64,731 high-quality cells were analyzed, comprising 35,537 GF and 29,194 SPF cells. Using cluster analysis and annotation, 10 distinctive cell clusters were identified and labeled as epithelial, T/NK cell, fibroblast, B cell, myeloid, smooth muscle cell (SMC), lymphatic endothelial cell (LEC), endothelial, terminal glial cell, and mesothelial cell (Figure 2A). Upon examination of cellular ratios, it was noted that the proportion of epithelial and fibroblast cells increased in GF mice, while the proportion of T/NK cells and B cells decreased (Figure 2B). In addition, each cell type exhibits its own distinct and unique marker genes<sup>24–28</sup> (Figure 2C).

In order to understand which cell types are mainly affected by microbial deletion, we conducted a statistical analysis of the number of differential genes in the cecum of GF and SPF mice, and found that the more concentrated groups of differential genes in the cecum of GF and SPF mice were mesenchymal cells and immune cells. The results indicate that microorganisms have a greater influence on the activity of mesenchymal and immune cells (Figure 2D).

### Spatial transcriptomic landscape of GF and SPF mouse cecum

In order to characterize the spatial transcriptomic landscape under different intestinal microbiota conditions, we processed frozen cecum from GF and SPF mice using a subcellular resolution, centimeter-scale field of view Stereo platform.<sup>29</sup> After filtering out low-quality points, the final dataset consisted of 3,685 GF sample Bin50 spots and 7,786 SPF sample Bin50 spots, for a total of 11,471 individual high-quality points. Each Bin50 spot in the GF samples had an average of approximately 1,677 genes and 4,455 unique transcripts. Each Bin50 spot in the SPF samples had an average of approximately 602 genes and 2,199 unique transcripts (Figure S2B). To ascertain the spatial transcriptomic structure of the GF and SPF mouse cecum, we subjected the spatial transcriptome dataset to clustering using the BayesSpace method.<sup>30</sup> Our final outcomes delineated three fundamental transcriptomic landscapes, identifiable as the intestinal epithelial cell layer, the mixed layer, and the muscle layer, conforming to recognizable histological features (Figure 2E).

To identify the cell types present in each bin of the spatial transcriptome, we integrated single-cell transcriptome data to deconvolute spatial transcriptome data from GF and SPF mice.<sup>31</sup> Our final outcomes revealed that the mucosal layer of GF and SPF mice primarily consisted of enterocytes and goblet cells. Further, the lamina propria comprises mesenchymal and immune cells, while smooth muscle cells dominate the muscle layer. Ultimately, our data analysis accurately described the spatial distribution of cell types commonly found in the cecum (Figures 2F and 2G).

### Low activity of extracellular matrix organization pathway is associated with cecal mucosal layer thinning

Significant anatomical differences were observed in the cecum of GF mice compared to SPF mice, with one notable change being the thinning of the mucosal layer of the GF cecum (Figures 1B–1E). Mesenchymal cells represent a crucial cell type underlying the structural integrity of the gut.<sup>32</sup> Considering the significant changes in the cecum phenotype of GF mice, the proportion and function of the mesenchymal cells may have changed significantly. Therefore, we focused on the mesenchymal cells of the GF and SPF cecum. There are three types of mesenchymal cells in our data, fibroblast (*Gsn* high), fibroblast (*Adamdec1* high), and mesothelial cell (Figure 3A). All three cell subclasses perform extracellular matrix tissue building functions, suggesting that mesenchymal cells are a key cell type in the structure of the cecum (Figure 3B). In addition, fibroblast (*Gsn* high) cells mainly perform extracellular matrix organization and extracellular structural organization (Figure 3B), fibroblast (*Adamdec1* high) cells mainly perform epithelial cell proliferation and epithelial tube morphogenesis, while mesothelial cells perform a

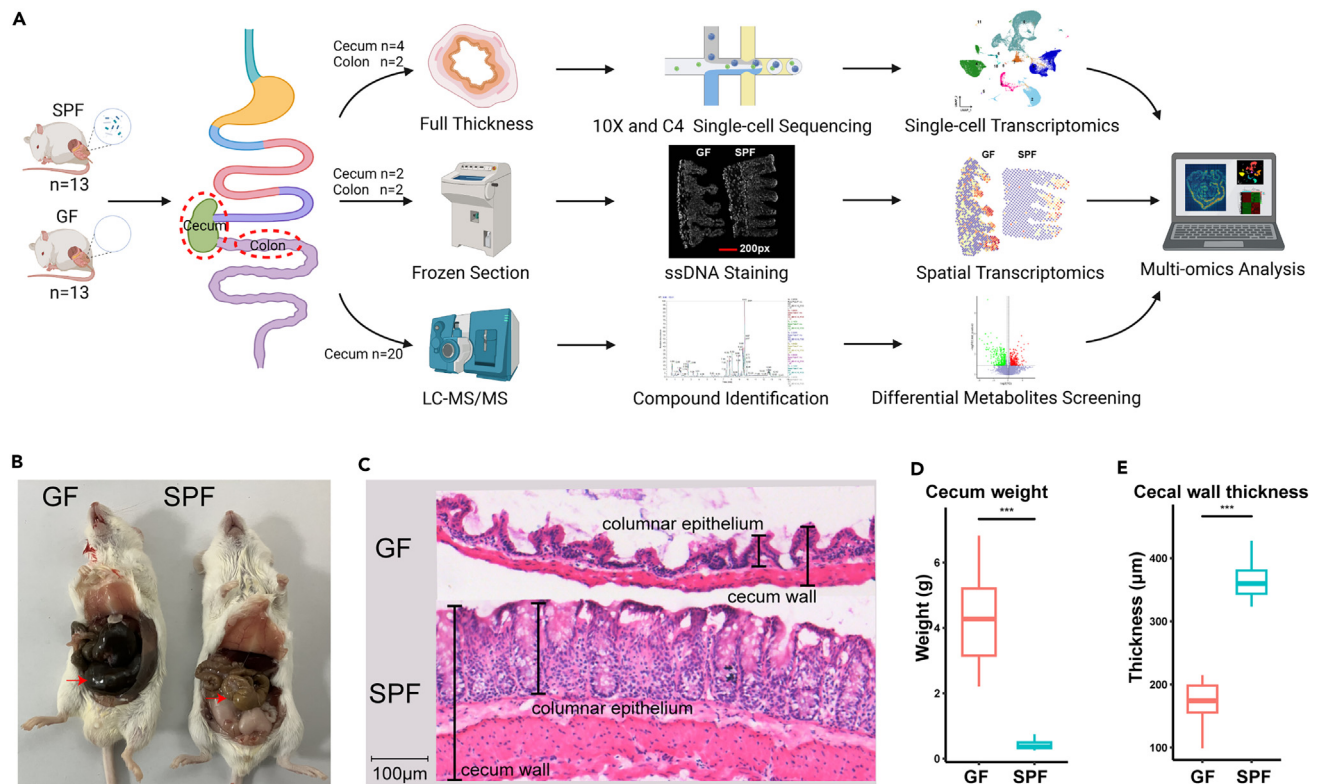


**Figure 1. Significant anatomical changes occur in the cecum of GF mice**

(A) Experimental design.

(B) Anatomical view of the cecum of GF and SPF mice showing the significantly enlarged cecum of GF mice. GF mice are shown on the left and SPF mice are shown on the right.

(C) H&E stained image showing significant wall thinning in the cecum of GF mice. The top of the image shows the GF cecum and the bottom of the image shows the SPF cecum. Resolution: 100  $\mu$ m.

(D) The cecum of GF mice weighs 9 times more than that of SPF mice. p values were generated by Student's t test. \*\*\* indicates  $p < 0.001$ .

(E) The thickness of the cecum wall of GF mice is one-third that of SPF mice. p values were generated by Student's t test. \*\*\* indicates  $p < 0.001$ .

more comprehensive range of functions. Spatially, fibroblast (*Gsn* high) cells are mainly found in the submucosa and muscle layer, which correlates with their structural building functions (Figures 3C and 3D). Fibroblast (*Adamdec1* high) cells are mainly found in the mucosal layer close to the epithelium, which correlates with their functions such as epithelial cell proliferation and epithelial tube morphogenesis. Mesothelial cells are found in the mucosal, submucosal and muscular layers, which is related to the more comprehensive functions they perform.

The results of the differential analysis of mesenchymal cells showed that GF mice had a reduced proportion of fibroblast (*Adamdec1* high) and an increased proportion of fibroblast (*Gsn* high) compared to SPF mice (Figure 3E). To gain a deeper insight into the functional modifications in GF mice, we performed GO (Gene Ontology) functional enrichment of differentially expressed genes in mesenchymal cells. Our analysis showed that pathways associated with extracellular matrix organization was reduced in fibroblasts from GF mice, suggesting that mesenchymal cells from GF mice have a reduced structural building function, which also correlates with the thinning of the mucosal layer (Figure 3F). Interestingly, we found that GF mouse cells showed increased activity in response to unfolded proteins (Figures 3F and S3E–S3G). This could imply nutritional deficiency due to microbiota deficiency and thus endoplasmic reticulum stress.

Mesenchymal cells have cellular regulatory functions in addition to their structural support functions.<sup>33,34</sup> In the statistics of cellular interactions, mesenchymal cell types were the strongest cell types for cellular interactions<sup>35</sup> (Figure S3A). Overall, the intensity of cellular interactions was significantly lower in the cecum of GF mice compared to SPF mice (Figure S3B). Comparing the interactions between cells from SPF mice and GF mice, we found that the differences were mainly in mesenchymal cell types, including fibroblast (*Adamdec1* high), fibroblast (*Gsn* high) and mesothelial (Figure S3C). Information flow indicates that most cellular interaction pathways are reduced in intensity in the GF cecum, such as GALECTIN, MK, ANGPTL, NCAM, MHC-II, MHC-I, and CD22 (Figure S3D). These results suggest that the regulatory function of GF cecal mesenchymal cells is decreased.

In summary, the absence of microorganisms significantly affects the structure-building and regulatory functions of the mesenchymal cells of the cecum. The thinning of the mucosal layer of the GF cecum corresponds to a significant reduction in the extracellular matrix organization of the mesenchymal cells.

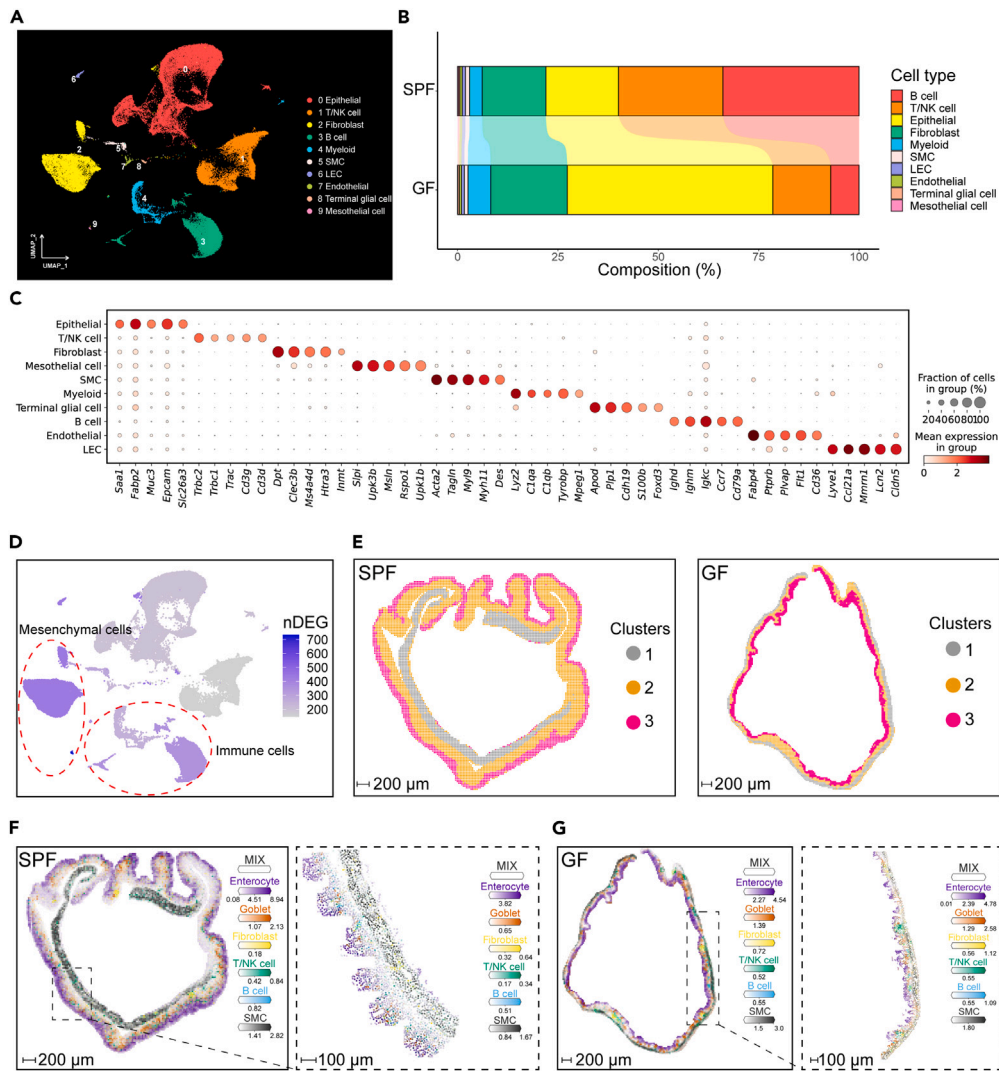


**Figure 2. Overview of single cell transcriptome and spatial transcriptome data from GF and SPF cecum**

(A) UMAP plot shows the ten main cell types of the cecum. SMC, smooth muscle cell; LEC, lymphatic endothelial cell.

(B) Proportion of cells in each cluster of GF and SPF cecum single cell transcriptome.

(C) Expression of marker genes in each cell type of cecum. Each dot represents a gene, where color saturation indicates the average expression level in the intestinal segment and size indicates the percentage of cells expressing the gene.

(D) The number of differential genes indicates that mesenchymal cells, immune cells have more differential genes. Color saturation indicates the number of differential genes. To find differential genes, the "FindMarkers" function in the seurat package was used, and the method used was "MAST." The screening conditions for highly expressed genes in GF mice were  $P_{\text{adjust}} < 0.05$ ,  $\text{avg}_{\text{log2FC}} > 0.58$ ,  $\text{log2FC} > 0.58$ . The screening conditions for highly expressed genes in SPF mice were:  $P_{\text{adjust}} < 0.05$ ,  $\text{avg}_{\text{log2FC}} < -0.58$ .

(E) BayesSpace clustering results for GF and SPF mice. The left side of the image shows SPF mice. The right side of the image shows GF mice. Cluster1 represents the muscle layer, Cluster2 represents the mixed layer, and Cluster3 represents the epithelial layer. Spatial data adopts Bin50 resolution.

(F) Deconvolution results show the spatial distribution of major cell types in SPF mice. The image on the left shows the whole slice, spatial data adopts Bin50 resolution. The picture on the right shows a partial view, spatial data adopts cell-Bin resolution.

(G) Deconvolution results show the spatial distribution of major cell types in GF mice. The image on the left shows the whole slice, spatial data adopts Bin50 resolution. The picture on the right shows a partial perspective, spatial data adopts cell-Bin resolution.

### Increased proportion of GF cecum EC (*Saa1* high) cells

Epithelial cells are the predominant cell type in the gut and perform a wealth of cellular functions. To characterize the changes in epithelial cells in the GF cecum, we performed a finer clustering of epithelial cell types in the cecum. From the total single cell transcriptome data, we isolated 21,897 high quality epithelial cells, of which SPF mouse cecum had 5,101 epithelial cells and GF mouse cecum had 16,796 epithelial cells. These epithelial cells could be divided mainly into goblet, enteroendocrine cell (EEC), tuft, EC (*Hmgb2* high) (Enterocyte with high

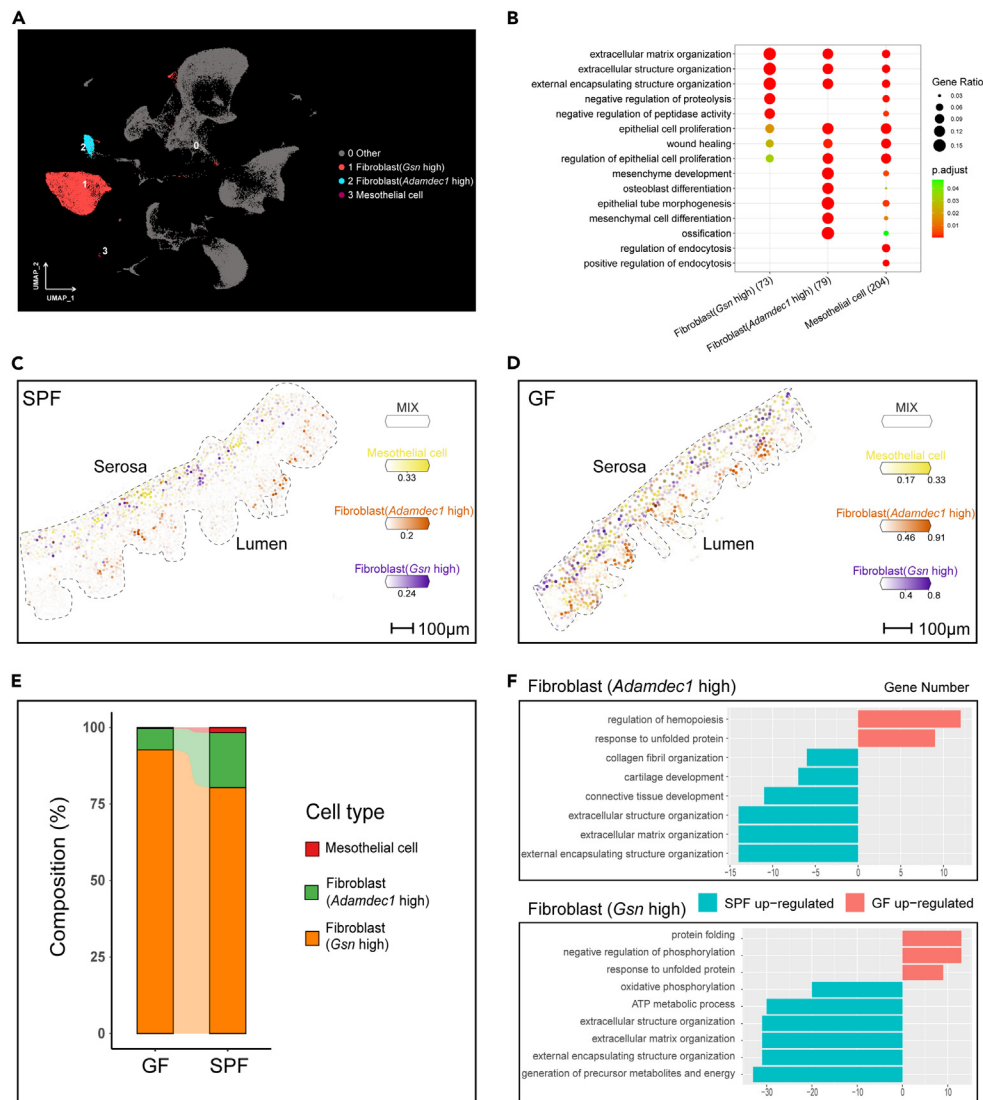


**Figure 3. Microbial defects significantly affect the structure-building function of mesenchymal cells**

(A) UMAP plot shows three major mesenchymal cell subtypes.

(B) GO enrichment results demonstrate that three mesenchymal cell subtypes perform different functions. Each dot indicates a pathway, where the color unsaturation indicates the level of p adjust and the size indicates the percentage of genes enriched to that pathway.

(C and D) Results of deconvolution of SPF and GF cecum mesenchymal cell subclasses. Fibroblast (*Adamdec1* high) cells are mainly found in the mucosal layer. Fibroblast (*Gsn* high) cells are mainly found in the submucosal and muscular layers. Mesothelial cells are found in the mucosal, submucosal and muscular layers. Results on the left show the SPF cecum (C). Results on the right show the GF cecum (D). Spatial data adopts cell-Bin resolution.

(E) The proportion of mesenchymal cells showed a significant increase in the proportion of fibroblast (*Gsn* high) cells.

(F) GO enrichment results demonstrate reduced activity in both subclasses of GF cecum mesenchymal cells in structurally constructed pathways. To find differential genes, the "FindMarkers" function in the seurat package was used, and the method used was "MAST." The screening conditions for highly expressed genes in GF mice were  $P_{\text{adjust}} < 0.05$ ,  $\text{avg}_{\text{log2FC}} > 0.25$ . The screening conditions for highly expressed genes in SPF mice were:  $P_{\text{adjust}} < 0.05$ ,  $\text{avg}_{\text{log2FC}} < -0.25$ . GO enrichment was performed on the results of differential genes, and the first few pathways with the most significant differences were selected for display.

expression of *Hmgb2* gene), EC (*Saa1* high), EC (*Selenbp1* high), EC (*Rpl3* high), EC (*Reg3b* high), EC (Dying) and mixed with a small number of mesenchymal lymphoid tissue organizer (mLT<sub>o</sub>) and Ep\_ Fibroblast (Figure 4A). We put marker gene of the different subclasses on display<sup>24–28</sup>(Figure 4B). There are five different sub-cell types of enterocytes.

One class of enterocytes with high *Saa1* expression, EC (*Saa1* high), has a significantly higher proportion of cells in the cecum of GF mice (Figure 4C). Compared with SPF mice, GF mice had more spots of high expression of *Saa1* gene (Figures 4D and S4A). Then, we deconvolute the spatial transcriptome data using the single cell data of the epithelial cells as the reference dataset.<sup>36</sup> We clearly found that EC (*Saa1* high),

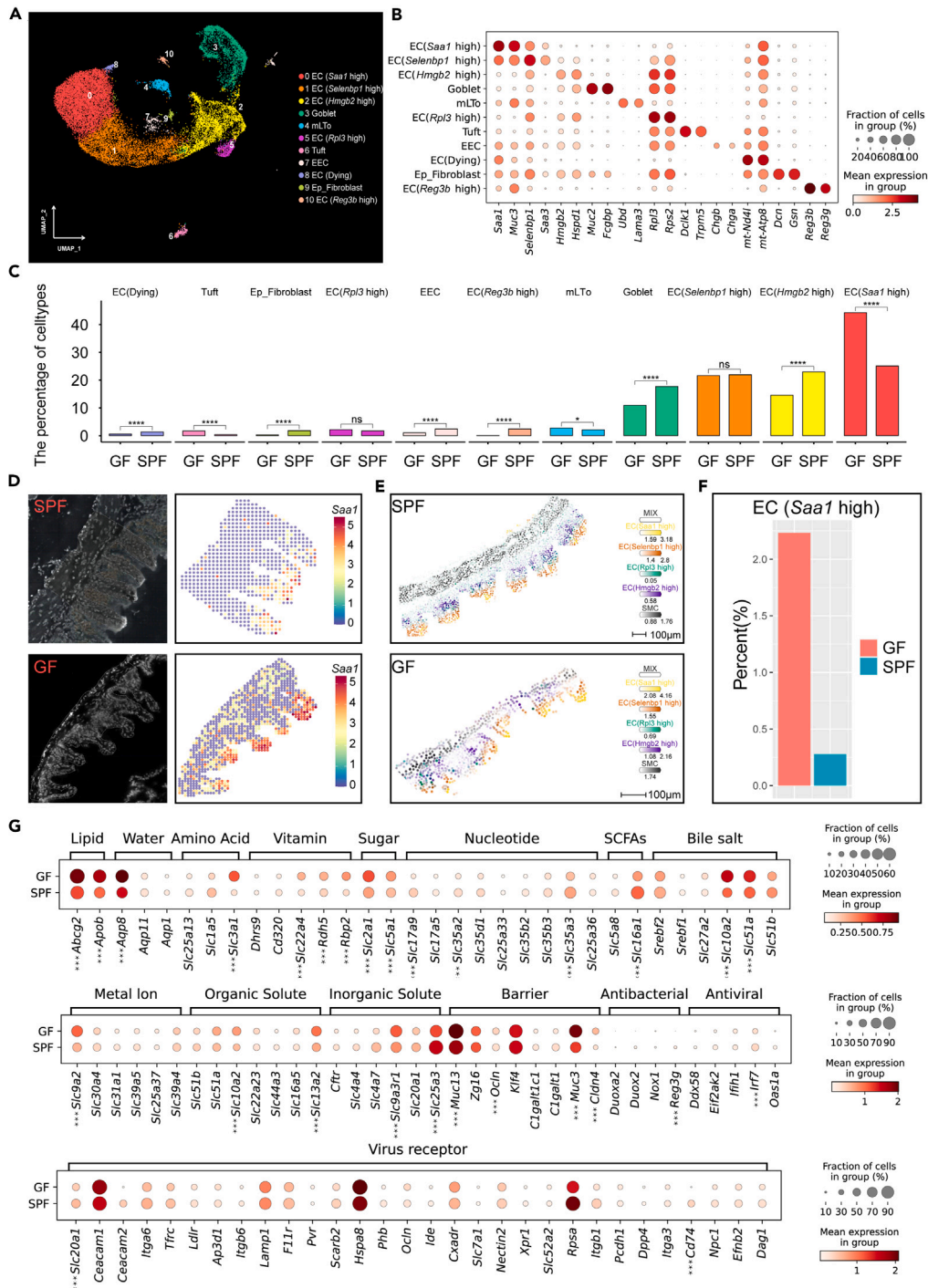


**Figure 4. Comparison of the single cell and spatial transcriptomes of cecum epithelial cells in GF and SPF cecum**

(A) UMAP plot shows 11 subtypes of cecum epithelial cells. EC, enterocyte; mLto, mesenchymal lymphoid tissue organizer; EEC, enteroendocrine cell.

(B) Expression of marker genes in each cell type of cecum epithelial cells.

(C) Significant increase in the proportion of GF cecum EC (Saa1 high) cells. p values were generated by Fisher's exact test. \*\*\*\* indicates p < 0.0001, \* indicates p < 0.05, ns means not significant.

(D) GF cecum has more spots with high expression of Saa1 gene. The ssDNA image is displayed on the left. Spatial data adopts Bin20 resolution.

(E) The enterocyte subtype is stratified along the columnar epithelium. Spatial data adopts cell-Bin resolution.

**Figure 4. Continued**

(F) Spatial transcriptome cell ratio results demonstrate an elevated proportion of EC (*Saa1* high) cells in the GF cecum.

(G) Enhanced water transport capacity and absorption of major nutrients in the cecum epithelium of GF mice. Each dot represents a gene, where color saturation indicates the average expression level in the intestinal segment and size indicates the percentage of cells expressing the gene. p values were generated by Wilcoxon test. \*\*\* indicates  $p < 0.001$ .

EC (*Selenbp1* high), EC (*Rpl3* high), and EC (*Hmgb2* high) were distributed in a layered manner from the top to the end of the columnar epithelium (Figures 4E and S4A–S4C). Subsequently, the proportion of EC (*Saa1* high) was counted on the spatial data. Spatial results showed that GF mice had a higher proportion of EC (*Saa1* high) cells compared with SPF mice (Figure 4F).

These findings indicate that the subclasses of enterocytes in the columnar epithelium of the cecum of both GF and SPF mice exhibit a layered distribution. Additionally, compared to SPF mice, GF mice display a larger proportion of EC (*Saa1* high) cells, accompanied by a broader spatial distribution.

**Increased water content in GF cecum correlates with high expression of *Aqp8* in epithelial cells**

Among the many remarkable changes in the cecum phenotype of GF mice compared with SPF mice, a notable feature is the significantly elevated water content in the GF mouse cecum. Previous studies have found similar phenomena.<sup>21</sup> To better comprehend the shift in water transport, we assessed several essential genes responsible for encoding water channel proteins in the mouse intestine. Interestingly, we observed a marked upregulation of the *Aqp8* water channel protein gene (Figure 4G). Spatial transcriptome and immunofluorescence result also showed that AQP8 protein expression was significantly upregulated in GF mice (Figures S4D–S4F and S5A). The AQP8 protein is a water channel protein, and altered osmotic gradients may be responsible for water enrichment in cecal contents. Therefore, we tested the total osmolality of cecum contents in GF mice. The results showed that the total osmolality of the cecum contents of GF mice was higher than that of physiological saline and did not change significantly relative to SPF mice (Table S1). Earlier studies have shown that accumulation of undegraded mucus and dietary carbohydrates at similar total osmolality results in high colloidal osmolality in the intestinal contents of GF rats, which may be responsible for the inhibition of water uptake.<sup>37</sup> When saline was used to replace the natural contents of the cecum of the GF animals in the *in vivo* experiments, the water uptake rate became normal or even higher than that of the conventional control group.<sup>38,39</sup> In addition, we found a significant decrease in the expression of *Aqp11* and *Aqp1* in the cecum of GF mice (Figures S5D–S5F), and because of the low expression of these two proteins in cecal epithelial cells, their changes may have a limited effect on water transport. In summary, the significant increase in AQP8 in epithelial cells is more likely to be responsible for the osmotic "secretion" of water into the lumen of the cecum.

**Absence of microorganisms enhances the nutrient absorption function of epithelial cells**

The cecum is an essential site for food fermentation, nutrient metabolism, and short-chain fatty acid production within the intestinal system, closely tied to the intestinal microbiota. Our study indicated significant alterations in the nutrient absorption capacity of the cecum in GF mice. Specifically, we noted significant upregulation in the transport of lipids, amino acids, vitamins, sugars, bile salts, metal ions, and organic and inorganic substances, while the transport of nucleotides and short-chain fatty acids was significantly reduced (Figure 4G; Table S2).

Enterocytes are the main cell type that performs nutrient absorption, and each subtype of cecum enterocyte performs a different function. For example, EC (*Saa1* high) cells mainly perform anion transport, unsaturated fatty acid metabolic process, EC (*Selenbp1* high) mainly perform steroid metabolic process, etc. (Figure S6A). To gain more insight into the effects of microbial deletion on epithelial cells, we performed differential analysis of multiple subtypes of epithelial cells (Figure S6B). Our results showed that EC (*Saa1* high) cells of the GF cecum increased the activity of the primary amino compound metabolic process, the vitamin metabolic process (Figure S6C). EC (*Selenbp1* high) cells of the GF cecum increased the activity of icosanoid metabolic process, unsaturated fatty acid metabolic process (Figure S6D). In addition, we analyzed the metabolic activity of cecum epithelial cells.<sup>40</sup> The results showed that EC (*Selenbp1* high) cells showed significantly increased activity in the pathways of tryptophan metabolism, unsaturated fatty acid biosynthesis and glycolysis (Figure S7A). In conclusion, these results suggest that microbial deficiency enhances the uptake and metabolic activity of key nutrients by epithelial cells.

**Microbial deficiency suppresses the immune function of epithelial cells**

Enterocytes not only perform nutrient absorption functions but also play an important role in intestinal immunity. Our results show that GF enterocyte subtypes have reduced immune activity in different ways compared to SPF enterocytes. For example, EC (*Saa1* high) cells were less active in the antigen processing and presentation of exogenous antigen pathway and EC (*Selenbp1* high) cells were less active in the defense response to bacterium pathway (Figures S6C and S6D). In addition, we focused on several major antimicrobial and antiviral genes of host epithelial cells as well as some enterovirus receptor genes (Figure 4G). Our results found that most antibacterial and antiviral genes as well as viral receptor genes were significantly downregulated in epithelial cells, indicating that antibacterial and antiviral strength and interactions were weakened.

**Microbial deletion inhibits the development of lymphoid glands**

We found a cluster of mesenchymal lymphoid tissue-organizer (mLTo) cells during the subclustering process of epithelial cells, which mainly perform functions such as response to molecule of bacterial origin, regulation of inflammatory response, and cell-substrate adhesion

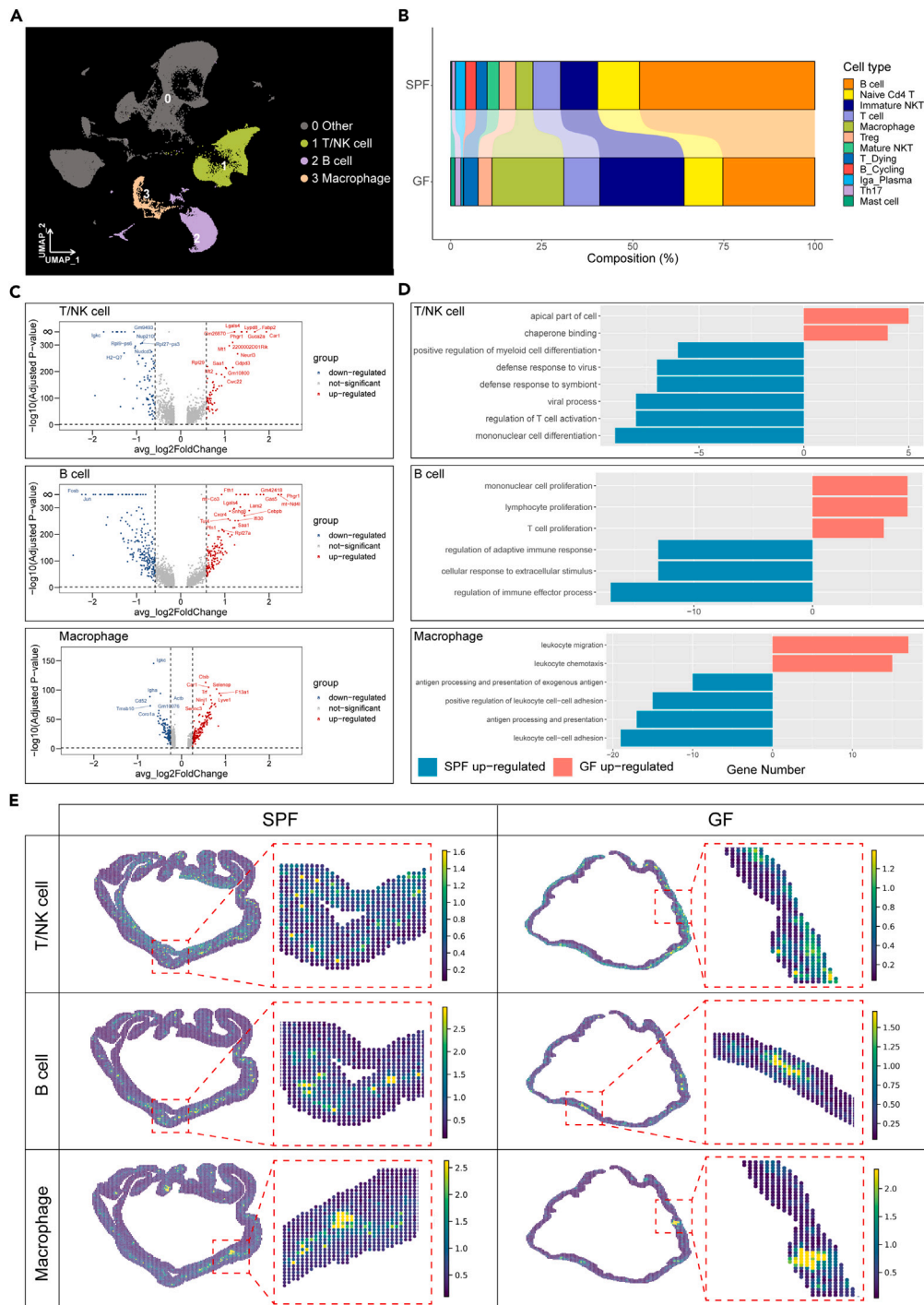


**Figure 5. Absence of microorganisms significantly impairs the proportion and function of immune cells**

(A) UMAP plot shows three main immune cell types.

(B) Mature NKT, Iga\_Plasma and other mature immune cells are significantly reduced in the proportion of GF cecum.

(C) Volcano map of differentially expressed genes in immune cells. To find differential genes, the "FindMarkers" function in the seurat package was used, and the method used was "MAST." The screening conditions for highly expressed genes in B cells and T/NK cells of SPF mice are  $P_{\text{adjust}} < 0.05$ ,  $\text{avg\_log}_2\text{FC} > 0.58$ . The screening conditions for highly expressed genes in B cells and T/NK cells of SPF mice are  $P_{\text{adjust}} < 0.05$ ,  $\text{avg\_log}_2\text{FC} < -0.58$ . The screening conditions for highly expressed genes in macrophage of GF mice are  $P_{\text{adjust}} < 0.05$ ,  $\text{avg\_log}_2\text{FC} > 0.25$ . The screening conditions for highly expressed genes in macrophage of SPF mice are  $P_{\text{adjust}} < 0.05$ ,  $\text{avg\_log}_2\text{FC} < -0.25$ .

**Figure 5. Continued**

(D) GO enrichment plot shows decreased immune function in three major immune cells. GO enrichment was performed on the results of differential genes, and the first few pathways with the most significant differences were selected for display.

(E) Results of immune cell deconvolution, showing the spatial distribution of immune cells in the cecum of GF and SPF mice. Local enlargements are shown in red boxes. Spatial data adopts Bin50 resolution.

(Figures S6A and S6F). Differential analysis between GF and SPF cecum showed that mLTo cells from GF mice had lower activity in gland development and positive regulation of cell adhesion pathway. In both GF and SPF cecum spatial transcriptome data, we found aggregation of mLTo cells near lymph nodes (Figures S6G and S6H). These results suggest that microbial deficiency affects the normal function of mLTo cells and inhibits the normal development of cecum lymph glands.

**Deficiency of microorganisms significantly affects the maturation of immune cells in the cecum**

The intestine harbors a diverse range of immune cell types that serve to safeguard the host from the intricate and varied foreign materials and microbial environment of the intestine.<sup>41</sup> To gain better insights into the overall changes in immune cells of GF mouse cecum, we focused on immune cell types in SPF and GF mice. Our data captured 26,685 high-quality immune cells, with 17,775 immune cells in SPF mice and 8,910 in GF mice, primarily composed of myeloid-lineage cells, B-lineage cells, and T/NK-lineage cells (Figure 5A). The main myeloid-lineage cells were macrophages and mast cells, while the main B-lineage cells comprised B cell, B\_Cycling, and Iga\_Plasma. T/NK-lineage cells exhibited several additional subtypes (Figure S2A).

To obtain a more complete understanding of T/NK-lineage cell subtypes, we further sub-clustered T/NK-lineage cells (Figure S8A). Seven known T/NK-lineage cell types were finally identified: Treg (*Foxp3*, *Tigit*, *Tnfrsf4*), naive Cd4 T (*Ccr7*, *Sell*, *Cd4*), Th17 (*Il22*, *Ccr6*, *Rora*), immature NKT (*Cd3g*, *Cd160*, *Cd7*), T cell (*S100a4*, *Ifng*, *S100a6*), T\_Dying (*mt-Co2*, *mt-Nd4*, *mt-Co1*), and mature NKT (*Gzma*, *Gzmb*, *Nkg7*) (Figure 7B). The main difference between mature NKT cells and immature NKT is the expression of the *Gzma* and *Gzmb* genes (Figure S8A).

We found that the proportion of mature NKT cells in the cecum of GF mice was very low relative to SPF mice. In addition, the proportion of mature B cells, Iga\_Plasma cells, were significantly reduced in GF mice (Figure 5B). It has been shown that the microbiota in the normal cecum plays a key role in maintaining immune homeostasis.<sup>42</sup> The decrease in mature immune cells indicates that the immune system maturation of GF mice is significantly impaired due to a lack of microorganisms.

**The immune function of immune cells in GF mice is inhibited**

To better comprehend the functional variances between immune cells, we conducted differential analyses of various immune cell types (Figure 5C). We then performed an enrichment analysis of these differential genes (Figure 5D), which illustrated pathways that were enriched in T/NK cells, B cells, and macrophages in SPF mice. Notably, these included immune cell differentiation, defense response to symbionts for T/NK cells, regulation of immune effector process, and regulation of adaptive immune response for B cells, along with leukocyte cell-cell adhesion and antigen processing and presentation pathways in macrophages. These outcomes suggest that the immune cells in GF mice may lack expression of related pathway genes. Furthermore, among T/NK cell subtypes, the *Cd3d* gene, involved in T cell development and signal transduction,<sup>43</sup> and the *Il22* gene, a member of the IL10 family of cytokines regulating cellular inflammatory responses.<sup>44</sup> *Il22* gene can also regulate the nutrient absorption ability and antibacterial ability of epithelial cells.<sup>45,46</sup> Interestingly, we found significant low expression of *Il22* in T cells and Cd4 T cells of GF mice (Figure S8D). These findings further highlight suppressed immune development, impaired immune function in GF mice.

To compare the spatial distribution of major immune cells and gain insights into the distribution bias of various immune cells in the GF and SPF cecum, we mapped single-cell transcriptome data of immune cells onto spatial sections<sup>36</sup> (Figures 5E, S8F, and S8G). Our findings revealed that T/NK cells in the cecum of both GF and SPF mice exhibited a predominantly homogeneous distribution pattern in the submucosa. Meanwhile, B cells and macrophages in the cecum of SPF mice showed a uniform, spaced pattern in the submucosal layer (Figures 5E, S8F, and S8G). By contrast, two small lymph node structures were visible in the GF mice sections, and B cells and macrophages were primarily distributed in these lymphatic structures (Figures 5E, S8F, and S8G).

**Absence of microorganisms affects metabolome homeostasis of cecum contents**

To gain insights into the changes in cecum content between GF and SPF mice, we collected cecum contents from ten GF mice and ten SPF mice. An LC-MS/MS platform was employed to conduct non-targeted metabolomic analysis. Overall, 1,969 metabolites were identified in cation mode and 967 metabolites in anion mode.

In order to discern the predominant enrichment pathways for these differential metabolites, we performed metabolic pathway enrichment analysis of the differential metabolites utilizing the KEGG (Kyoto Encyclopedia of Genes and Genomes) database. Our results indicated that GF mouse cecum contents in cation mode exhibited significant differences in metabolic pathways, including vitamin digestion and absorption, tryptophan metabolism, and cortisol synthesis and secretion (Figure 6A). Meanwhile, the anion mode displayed greater differences in metabolic pathways such as riboflavin metabolism and histidine metabolism (Figure 6B).

Cortisol and L-tryptophan metabolites were significantly enriched in the contents of the cecum of GF mice (Figure 6C). Cortisol is a stress hormone that exacerbates obesity and depression.<sup>47,48</sup> L-tryptophan is instrumental in regulating immunity, neuronal function, and intestinal

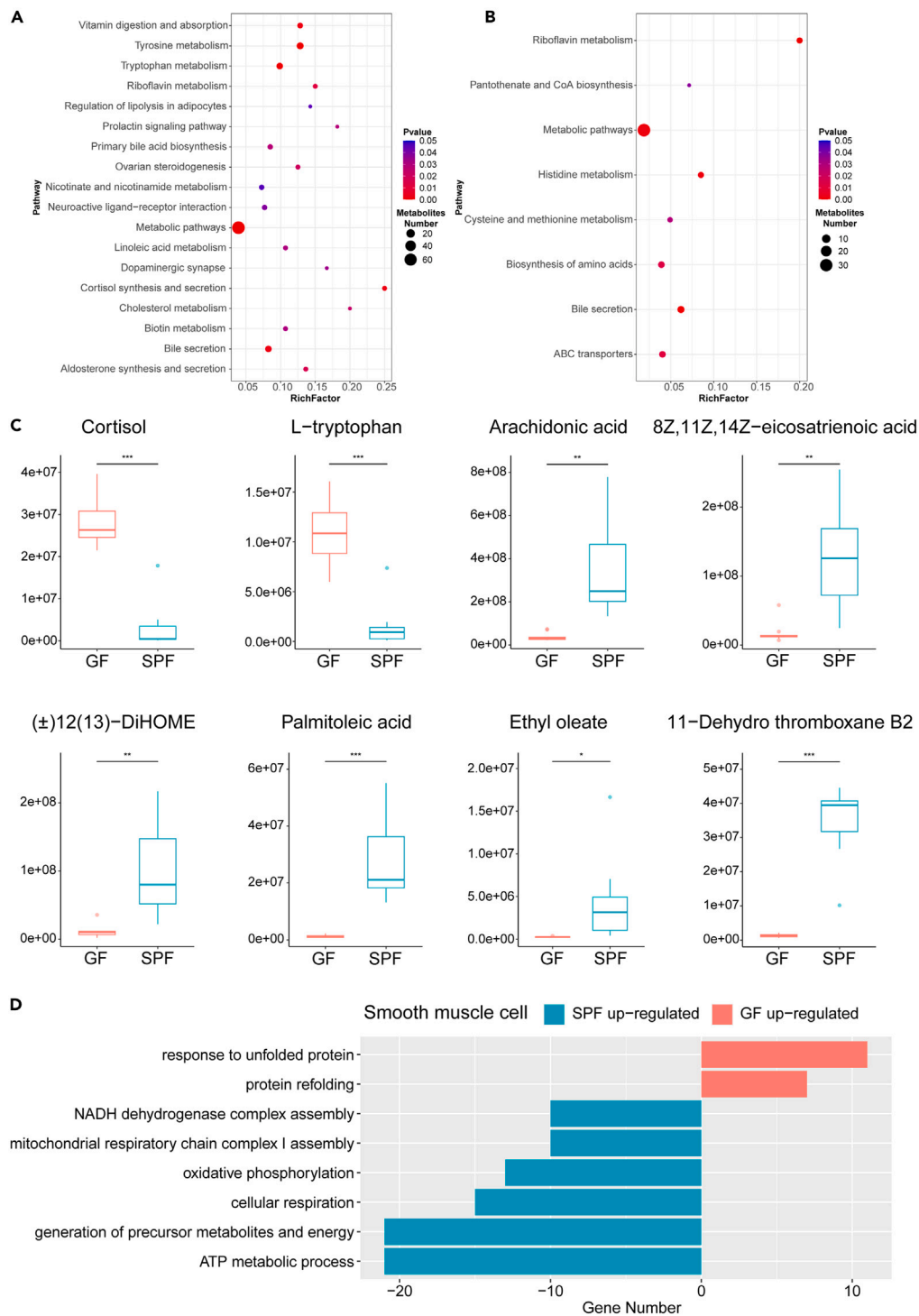


**Figure 6. Significant changes in the metabolism of cecal contents in GF mice compared to SPF mice**

(A) KEGG functional enrichment map of cationic differential metabolites in the cecal content metabolome of GF and SPF mice. The results showed significant differences in the metabolic pathways of vitamins, amino acids and cortisol. RichFactor is the number of differential metabolites annotated to the pathway divided by all identified metabolites annotated to the pathway. The dot size represents the number of differential metabolites annotated to this pathway.

(B) KEGG functional enrichment map of anionic differential metabolites in the cecal content metabolome of GF and SPF mice. The results showed significant differences in metabolic pathways such as riboflavin, amino acids and bile acids.

**Figure 6. Continued**

(C) Boxplot showing significantly changed metabolites in cecal contents of GF mice. The results showed that metabolites such as tryptophan and cortisol were significantly enriched in the GF cecum contents and unsaturated fatty acids such as arachidonic acid were significantly absent. p values were generated by Student's t test. \*\*\* indicates  $p < 0.001$ , \*\* indicates  $p < 0.01$ , \* indicates  $p < 0.05$ .

(D) Differential gene GO enrichment results demonstrate a significant decrease in GF cecum smooth muscle cell (SMC) activity. To find differential genes, the "FindMarkers" function in the seurat package was used, and the method used was "MAST." The screening conditions for highly expressed genes in GF mice were  $P_{\text{adjust}} < 0.05$ ,  $\text{avg}_{\text{log2FC}} > 0.25$ . The screening conditions for highly expressed genes in SPF mice were:  $P_{\text{adjust}} < 0.05$ ,  $\text{avg}_{\text{log2FC}} < -0.25$ . GO enrichment was performed on the results of differential genes, and the first few pathways with the most significant differences were selected for display.

homeostasis through the kynurenine metabolic pathway (KP).<sup>49</sup> Aberrant metabolism of L-tryptophan impairs immune function and disrupts intestinal homeostasis.<sup>50</sup>

Unsaturated fatty acids can be categorized into monounsaturated fatty acids and polyunsaturated fatty acids, depending on their number of double bonds. A wealth of literature supports the notion that unsaturated fatty acids play a significant role in disease and health in mammals.<sup>51–55</sup> Our analysis revealed that unsaturated fatty acid-related metabolites, including arachidonic acid, 8Z,11Z,14Z–eicosatrienoic acid, ( $\pm$ )12(13)–Di-HOME, palmitoleic acid, ethyl oleate, and 11–dehydro thromboxane B2 were significantly reduced in the cecum contents of GF mice (Figure 6C). Notably, arachidonic acid is known to be involved in muscle activity,<sup>56</sup> and our data also demonstrated reduced SMC activity in the cecum of GF mice (Figure 6D). These results predict reduced motility in the GF cecum. Interestingly, an earlier study found reduced colonic motility in GF mice.<sup>57</sup> The lower motility of the cecum, a sac-like organ, may lead to a large accumulation of contents, ultimately leading to a larger cecum.

**Functional changes in colonic cells in a microbial deficient state**

Although we understand the significant functional changes that occur in the cecum of GF mice, it is unclear whether the same changes occur in other intestinal segments of GF mice. For this reason, we have compared the colon of GF and SPF mice. Interestingly, the epithelial cell subtype of the colon was also stratified along the columnar epithelium (Figure 7A). EC (*Atp12a* high) cells, which are distributed at the apical part of the columnar epithelium and perform mainly intestinal absorption and ion transport functions, also have a significantly higher proportion of cells in the GF colon. (Figures 7B and 7C). Notably, functional genes that were significantly altered in the GF cecum epithelium were similarly altered in the GF mouse colon. For example, the lipid uptake genes *Abcg2*, *Apob*, the water channel gene *Aqp8*, the intestinal barrier function-related genes *Muc3*, *Cldn4*, the amino acid transporter gene *Slc3a1*, the sugar transporter gene *Slc2a1*, and the bile acid salt transporter gene *Slc10a2* all showed significantly elevated expression in the GF colon epithelium (Figure 7D). The expression of the short-chain fatty acid transporter protein gene *Slc16a1* and the antimicrobial protein gene *Reg3b* was significantly decreased in GF colonic epithelial cells (Figure 7D). In addition, we also found significant low expression of the *Il22*, *Cd3d* gene in colonic T cells, indicating that immune development and immune function of GF colonic T cells were also significantly suppressed (Figure 7E). Furthermore, in GF colonic fibroblasts, we similarly observed a lack of functions such as extracellular structure building (Figure 7F). An earlier study found thinning of the mucosal layer of the colon in GF mice.<sup>58</sup> Interestingly, we observed a significant thinning of the mucosal layer of the GF colon (Figure 7G). Overall, the functional changes in GF mouse colon cells in the microbial deficient state were consistent with those in the cecum.

**DISCUSSION**

In this study, we used single-cell transcriptomic, spatial transcriptomic, and metabolomic techniques to characterize and compare differences between GF and SPF mice and to decipher the structural and functional effects of the gut microbiota on the large intestine at a multi-omics level.

We counted in detail the phenotypic differences between the cecum of GF and SPF mice. Valuable insights from multiple earlier studies support our anatomical observations.<sup>21,22,59,60</sup> In addition, there is a strong association between microbes and mesenchymal cells in the large intestine. The absence of microbes has a tremendous impact on mesenchymal cells. However, the mechanisms of interactions between microbes and mesenchymal stromal cells are unknown and need to be further explored in the future.

Earlier studies found that AQP8 may be involved in the cytoplasmic condensation that occurs during the differentiation of spermatocytes into spermatozoa as well as in the production of seminiferous tubule fluid.<sup>61</sup> More recent studies have found an association between the AQP8 protein and excess amniotic fluid.<sup>62,63</sup> Furthermore, in addition to being a water channel, AQP8 is permeable to hydrogen peroxide. Hydrogen peroxide is not only an ROS (Reactive oxygen species) but also an important signaling molecule. In general, AQP must be regarded as a putative participant in oxidative stress situations.<sup>64</sup> Therefore, an increase in AQP8 protein may have potential effects on metabolite-host interactions in addition to affecting intestinal water transport function. In addition, we found that *Aqp11* and *Aqp1* expression in the cecum of GF mice decreased significantly with increasing *Aqp8*. *Aqp8* is expressed mainly in EC (*Saa1* high) cells, and *Aqp11* and *Aqp1* are expressed mainly in other epithelial cells, and the corresponding expression ratios of the water transport proteins are affected as the proportions of these cell types are varied in GF mice.

Despite the reduced motility of the GF colon muscles, the GF colon did not become as significantly larger as the cecum. We suggest that due to the special structure of the cecum, the relatively closed space inside the cecum, and the reduced peristaltic capacity of the muscles, the cecum can easily accumulate water and inclusions inside the cecum, which ultimately leads to more significant anatomical changes in the cecum.

Earlier studies have shown that differences in diet lead to epithelial cell remodeling, suggesting that nutrients affect epithelial cells.<sup>45</sup> Our study was conducted under the same nutritional conditions, suggesting that microorganisms have a similarly significant effect on epithelial cell proportions and function. Combined with the significant changes in the metabolic composition of GF cecum contents, we suggest that microbial deficiency may indirectly affect epithelial cell proportions and function through changes in metabolic composition. A recent study

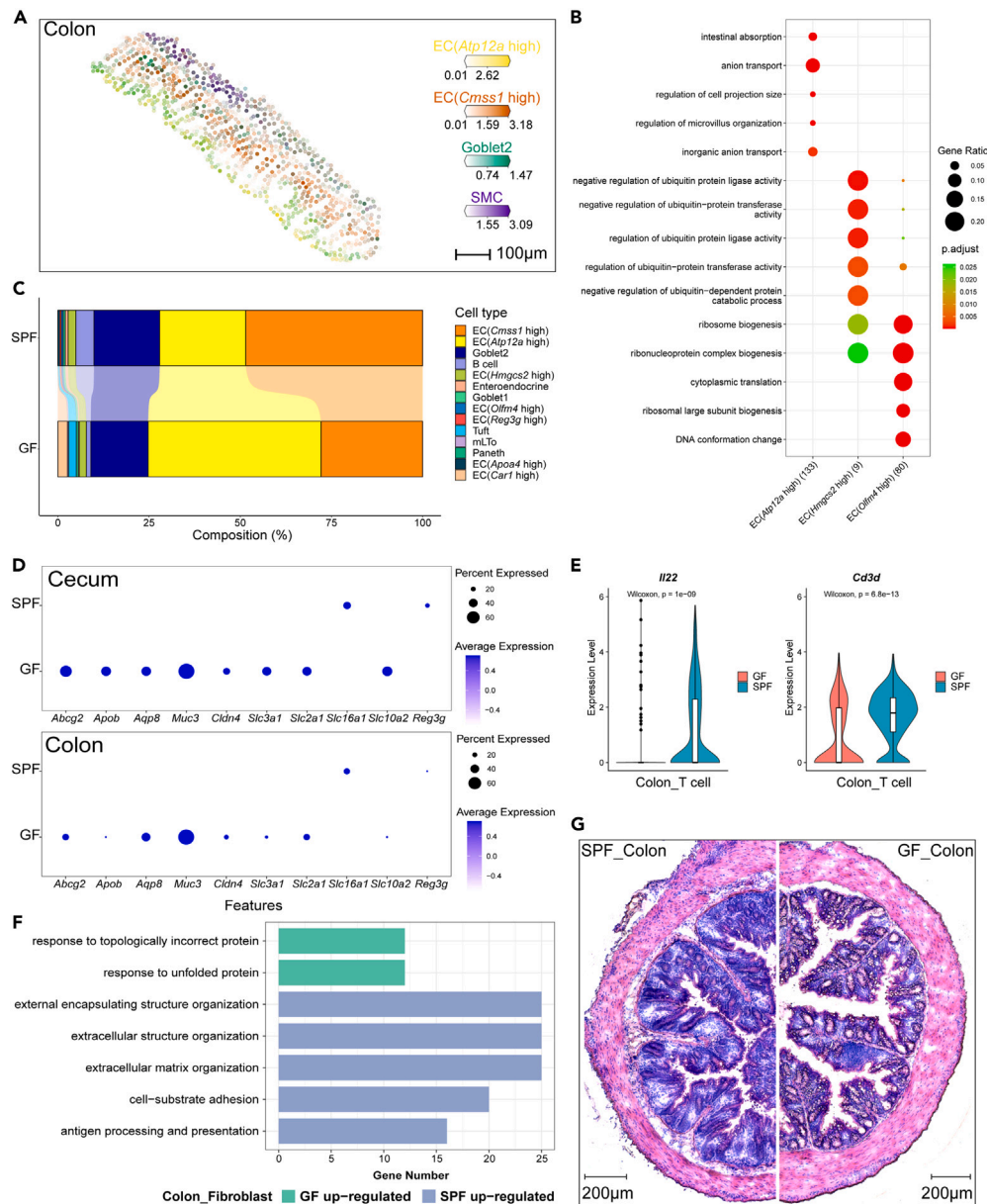


**Figure 7. Effect of microbial deficiency on colonic cell function**

(A) Deconvolution results show that subclasses of colonic epithelial cells are stratified along the columnar epithelium. EC, enterocyte; SMC, smooth muscle cell.

(B) GO enrichment results demonstrate that colonic epithelial cell subtypes perform distinct cellular functions. Each dot indicates a pathway, where the color unsaturation indicates the level of p adjust and the size indicates the percentage of genes enriched to that pathway.

(C) The proportion of colon epithelial cells in GF and SPF mice. The proportion of EC (*Atp12a* high) cells located in the apical mucosal layer of the colon was significantly higher in the GF colon.

(D) Enhanced water transport capacity and absorption of major nutrients in the cecum and colonic epithelium of GF mice. Each dot represents a gene, where color saturation indicates the average expression level in the intestinal segment and size indicates the percentage of cells expressing the gene.

(E) Differential expression of *Il22* and *Cd3d* genes in colon T cells of GF and SPF mice.

(F) GO enrichment results show reduced structure-building function of colonic fibroblasts. To find differential genes, the "FindMarkers" function in the seurat package was used, and the method used was "MAST." The screening conditions for highly expressed genes in GF mice were  $P_{\text{adjust}} < 0.05$ ,  $\text{avg}_{\text{log2FC}} > 0.25$ . The screening conditions for highly expressed genes in SPF mice were:  $P_{\text{adjust}} < 0.05$ ,  $\text{avg}_{\text{log2FC}} < -0.25$ . GO enrichment was performed on the results of differential genes, and the first few pathways with the most significant differences were selected for display.

(G) H&E staining of the colon of GF and SPF mice. The mucosal layer of the colon was significantly thinner in GF mice compared to SPF mice.

showed that T cells can inhibit *Il22* expression in mice, leading to activation of digestive enzymes and nutrient transport proteins by epithelial cells.<sup>45</sup> Another study reported that inhibition of *Il22* expression by ILC3 enhances lipid uptake by intestinal epithelial cells but reduces the expression of antimicrobial peptides.<sup>46</sup> Interestingly, our data suggest that *Il22* expression in Cd4 T cells from GF mice was significantly reduced. Data from GF colonies also showed a significant reduction in *Il22* expression in T cells. Based on these findings, we hypothesized that microbial deficiency in GF mice could enhance nutrient uptake in epithelial cells by inhibiting *Il22* expression in Cd4 T cells.

Gut microbes and their metabolites play a key role in the regulation of various immune cells.<sup>65–68</sup> Our results suggest that microbial deficiencies lead to significant suppression of immune function and immune cell maturation. Earlier studies also support our observations.<sup>69</sup>

Our findings elucidate the reasons for the significant anatomical changes observed in the cecum of GF mice and demonstrate the influence of the gut microbiota on large intestine structure and function. A key strength of our study is the integration of multi-omics data, which provides a comprehensive understanding of the differences between GF and SPF mice from multiple perspectives. Our findings suggest that microorganisms play an important role in shaping the morphological structure, cellular function, and cellular distribution of the host intestine. However, the effects of microbiota on other intestinal segments, and which microbiota defects are important for host structure and function, need to be further explored. Our study is the first multi-omics study of the GF large intestine and fills a research gap in the field of GF mice. Our findings provide a new and potentially critical reference point for future studies on the impact of the microbiota on the host gut.

### Limitations of the study

Our study identified several limitations. First, the mice used in our study were male and the effect of sex was not assessed. Secondly, biological replication and experimental validation may be required to draw definitive biological conclusions. Finally, although our study was able to understand the changes in the structural function of the large intestine of mice in a completely sterile state, it was not possible to understand the effects of specific strains of bacteria on the structure and function of the intestine.

### STAR★METHODS

Detailed methods are provided in the online version of this paper and include the following:

- KEY RESOURCES TABLE
- RESOURCE AVAILABILITY
  - Lead contact
  - Materials availability
  - Data and code availability
- EXPERIMENTAL MODELS AND STUDY PARTICIPANT DETAILS
  - Mouse rearing
  - Ethics approval
- METHOD DETAILS
  - Single cell transcriptome sample processing and sequencing
  - Spatial transcriptome sample processing and sequencing
  - Sample preparation and data analysis for non-targeted metabolome
- QUANTIFICATION AND STATISTICAL ANALYSIS
  - Single cell data pre-processing
  - Analysis of cellular interactions
  - Analysis of cellular metabolic activity
  - Spatial data pre-processing
  - Spatial clustering
  - Deconvolution
  - Statistics and reproducibility
  - Immunofluorescence
  - Total osmolality determination

### SUPPLEMENTAL INFORMATION

Supplemental information can be found online at <https://doi.org/10.1016/j.isci.2024.108941>.

### ACKNOWLEDGMENTS

We sincerely thank Jingjing Ye, Zidong Fang, Zishan Wang, Yunqiu Wang, Feng Kui and Wen Zhuang for their support of the experimental process. We are grateful to Wei Peng for his guidance on image beautification. We are also very grateful to BioRender for supporting the project design drawings.

Funding: This work was supported by the Science Technology and Innovation Committee of Shenzhen Municipality, China (SGDX20190919142801722).

## AUTHOR CONTRIBUTIONS

H.W. and X.F. designed the study. H.S., W.C., and H.Z. bred the mice. T.C., R.Z., L.W., and S.P. processed the samples in the laboratory. T.C., J.S., Y.S., Y.H., W.L., Z.Z., X.C., J.L., and H.Y. contributed to the data analysis. T.C. wrote the manuscript. J.S., Y.H., Y.C., X.H., Y.Z., L.H., and Q.Q. critically reviewed the manuscript. A.G. performed immunofluorescence experiments and osmolality experiments. H.W. and X.F. were responsible for the overall content as guarantors.

## DECLARATION OF INTERESTS

The authors declare no competing interests.

Received: June 27, 2023

Revised: November 3, 2023

Accepted: January 15, 2024

Published: January 17, 2024

## REFERENCES

- Hornbuckle, W.E., and Tennant, B.C. (1997). Gastrointestinal function. In *Clinical biochemistry of domestic animals* (Elsevier), pp. 367–406.
- Baumgart, D.C., and Dignass, A.U. (2002). Intestinal barrier function. *Curr. Opin. Clin. Nutr. Metab. Care* 5, 685–694. <https://doi.org/10.1097/00075197-200211000-00012>.
- Li, Z., Hao, M.M., Van den Haute, C., Baekelandt, V., Boesmans, W., and Vanden Berghe, P. (2019). Regional complexity in enteric neuron wiring reflects diversity of motility patterns in the mouse large intestine. *Elife* 8, e42914.
- Eisenstein, M. (2016). Biology: A slow-motion epidemic. *Nature* 540, S98–S99. <https://doi.org/10.1038/540S98a>.
- Le, H.H., Lee, M.-T., Besler, K.R., Comrie, J.M.C., and Johnson, E.L. (2022). Characterization of interactions of dietary cholesterol with the murine and human gut microbiome. *Nat. Microbiol.* 7, 1390–1403.
- Pellegrini, C., Fornai, M., D'Antongiovanni, V., Antonioli, L., Bernardini, N., and Derkinderen, P. (2023). The intestinal barrier in disorders of the central nervous system. *Lancet. Gastroenterol. Hepatol.* 8, 66–80. [https://doi.org/10.1016/S2468-1253\(22\)00241-2](https://doi.org/10.1016/S2468-1253(22)00241-2).
- Holle, J., Bartolomaeus, H., Löber, U., Behrens, F., Bartolomaeus, T.U.P., Anandakumar, H., Wimmer, M.I., Vu, D.L., Kuhring, M., Brüning, U., et al. (2022). Inflammation in Children with CKD Linked to Gut Dysbiosis and Metabolite Imbalance. *J. Am. Soc. Nephrol.* 33, 2259–2275. <https://doi.org/10.1681/ASN.2022030378>.
- Hendriks, T., Lang, S., Rajcic, D., Wang, Y., McArdle, S., Kim, K., Mikulski, Z., and Schnabl, B. (2023). Hepatic pIgR-mediated secretion of IgA limits bacterial translocation and prevents ethanol-induced liver disease in mice. *Gut* 72, 1959–1970. <https://doi.org/10.1136/gutjnl-2022-328265>.
- Olofsson, L.E., and Bäckhed, F. (2022). The Metabolic Role and Therapeutic Potential of the Microbiome. *Endocr. Rev.* 43, 907–926. <https://doi.org/10.1210/endo/bnac004>.
- Clemente, J.C., Ursell, L.K., Parfrey, L.W., and Knight, R. (2012). The impact of the gut microbiota on human health: an integrative view. *Cell* 148, 1258–1270.
- Wong, S.H., and Yu, J. (2019). Gut microbiota in colorectal cancer: mechanisms of action and clinical applications. *Nat. Rev. Gastroenterol. Hepatol.* 16, 690–704. <https://doi.org/10.1038/s41575-019-0209-8>.
- Renz, H., Brandtzaeg, P., and Hornef, M. (2011). The impact of perinatal immune development on mucosal homeostasis and chronic inflammation. *Nat. Rev. Immunol.* 12, 9–23.
- Shin, S.C., Kim, S.-H., You, H., Kim, B., Kim, A.C., Lee, K.-A., Yoon, J.-H., Ryu, J.-H., and Lee, W.J. (2011). Drosophila microbiome modulates host developmental and metabolic homeostasis via insulin signaling. *Science* 334, 670–674.
- Hill, J.H., and Round, J.L. (2021). SnapShot: Microbiota effects on host physiology. *Cell* 184, 2796–2796.e1.
- Zhang, J., Lu, Y., Wang, Y., Ren, X., and Han, J. (2018). The impact of the intestinal microbiome on bone health. *Intractable Rare Dis. Res.* 7, 148–155. <https://doi.org/10.5582/irdr.2018.01055>.
- Zhao, L., Zhang, X., Zhou, Y., Fu, K., Lau, H.C.-H., Chun, T.W.-Y., Cheung, A.H.-K., Coker, O.O., Wei, H., Wu, W.K.K., et al. (2022). *Parvimonas micra* promotes colorectal tumorigenesis and is associated with prognosis of colorectal cancer patients. *Oncogene* 41, 4200–4210.
- Franzosa, E.A., Sirota-Madi, A., Avila-Pacheco, J., Fomelos, N., Haiser, H.J., Reinker, S., Vatanen, T., Hall, A.B., Mallick, H., McIver, L.J., et al. (2019). Gut microbiome structure and metabolic activity in inflammatory bowel disease. *Nat. Microbiol.* 4, 293–305.
- Henrick, B.M., Rodriguez, L., Lakshminanth, T., Pou, C., Henckel, E., Arzoomand, A., Olin, A., Wang, J., Mikes, J., Tan, Z., et al. (2021). Bifidobacteria-mediated immune system imprinting early in life. *Cell* 184, 3884–3898.e11. <https://doi.org/10.1016/j.cell.2021.05.030>.
- Trávníček, J., and Mandel, L. (1979). Gnotobiotic techniques. *Folia Microbiol.* 24, 6–10.
- Clench, M.H. (1999). The avian cecum: update and motility review. *J. Exp. Zool.* 283, 441–447.
- Savage, D.C., and Dubos, R. (1968). Alterations in the mouse cecum and its flora produced by antibacterial drugs. *J. Exp. Med.* 128, 97–110. <https://doi.org/10.1084/jem.128.1.97>.
- Al-Asmakh, M., and Zadjali, F. (2015). Use of Germ-Free Animal Models in Microbiota-Related Research. *J. Microbiol. Biotechnol.* 25, 1583–1588. <https://doi.org/10.4014/jmb.1501.01039>.
- Tilg, H., Adolph, T.E., Gerner, R.R., and Moschen, A.R. (2018). The intestinal microbiota in colorectal cancer. *Cancer Cell* 33, 954–964.
- Moor, A.E., Harnik, Y., Ben-Moshe, S., Massasa, E.E., Rozenberg, M., Eilam, R., Bahar Halpern, K., and Itzkovitz, S. (2018). Spatial reconstruction of single enterocytes uncovers broad zonation along the intestinal villus axis. *Cell* 175, 1156–1167.e15.
- Fawcner-Corbett, D., Antanaviciute, A., Parikh, K., Jagielowicz, M., Gerós, A.S., Gupta, T., Ashley, N., Khamis, D., Fowler, D., Morrissey, E., et al. (2021). Spatiotemporal analysis of human intestinal development at single-cell resolution. *Cell* 184, 810–826.e23.
- Elmentaite, R., Kumasaka, N., Roberts, K., Fleming, A., Dann, E., King, H.W., Kleshchevnikov, V., Dabrowska, M., Pritchard, S., Bolt, L., et al. (2021). Cells of the human intestinal tract mapped across space and time. *Nature* 597, 250–255. <https://doi.org/10.1038/s41586-021-03852-1>.
- Kim, J.E., Fei, L., Yin, W.C., Coquenlorge, S., Rao-Bhatia, A., Zhang, X., Shi, S.S.W., Lee, J.H., Hahn, N.A., Rizvi, W., et al. (2020). Single cell and genetic analyses reveal conserved populations and signaling mechanisms of gastrointestinal stromal niches. *Nat. Commun.* 11, 334. <https://doi.org/10.1038/s41467-019-14058-5>.
- Han, X., Wang, R., Zhou, Y., Fei, L., Sun, H., Lai, S., Saadatpour, A., Zhou, Z., Chen, H., Ye, F., et al. (2018). Mapping the mouse cell atlas by microwell-seq. *Cell* 172, 1091–1107.e17.
- Chen, A., Liao, S., Cheng, M., Ma, K., Wu, L., Lai, Y., Qiu, X., Yang, J., Xu, J., Hao, S., et al. (2022). Spatiotemporal transcriptomic atlas of mouse organogenesis using DNA nanoball-patterned arrays. *Cell* 185, 1777–1792.e21. <https://doi.org/10.1016/j.cell.2022.04.003>.
- Zhao, E., Stone, M.R., Ren, X., Guenther, J., Smythe, K.S., Pulliam, T., Williams, S.R., Uyttingco, C.R., Taylor, S.E.B., Nghiem, P., et al. (2021). Spatial transcriptomics at subspace resolution with BayesSpace. *Nat. Biotechnol.* 39, 1375–1384.
- Cable, D.M., Murray, E., Zou, L.S., Goeva, A., Macosko, E.Z., Chen, F., and Irizarry, R.A. (2022). Robust decomposition of cell type mixtures in spatial transcriptomics. *Nat. Biotechnol.* 40, 517–526.
- Pinchuk, I.V., Mifflin, R.C., Saada, J.I., and Powell, D.W. (2010). Intestinal mesenchymal

- cells. *Curr. Gastroenterol. Rep.* 12, 310–318. <https://doi.org/10.1007/s11894-010-0135-y>.
33. Wu, N., Sun, H., Zhao, X., Zhang, Y., Tan, J., Qi, Y., Wang, Q., Ng, M., Liu, Z., He, L., et al. (2021). MAP3K2-regulated intestinal stromal cells define a distinct stem cell niche. *Nature* 592, 606–610.
  34. Nagashima, K., Sawa, S., Nitta, T., Tsutsumi, M., Okamura, T., Penninger, J.M., Nakashima, T., and Takayanagi, H. (2017). Identification of subepithelial mesenchymal cells that induce IgA and diversify gut microbiota. *Nat. Immunol.* 18, 675–682.
  35. Jin, S., Guerrero-Juarez, C.F., Zhang, L., Chang, I., Ramos, R., Kuan, C.-H., Myung, P., Plikus, M.V., and Nie, Q. (2021). Inference and analysis of cell-cell communication using CellChat. *Nat. Commun.* 12, 1088.
  36. Kleshchevnikov, V., Shmatko, A., Dann, E., Aivazidis, A., King, H.W., Li, T., Elmentaite, R., Lomakin, A., Kedlian, V., Gayoso, A., et al. (2022). Cell2location maps fine-grained cell types in spatial transcriptomics. *Nat. Biotechnol.* 40, 661–671.
  37. Gordon, H.A., and Nakamura, S. (1975). Elevated levels of colloid osmotic pressure in cecal contents of germfree animals. *Proc. Soc. Exp. Biol. Med.* 149, 46–49.
  38. Gordon, H., and Wostmann, B. (1973). Chronic mild diarrhea in germfree rodents: a model portraying host-flora synergism. In *Germfree research* (Elsevier), pp. 593–601.
  39. Donowitz, M., and Binder, H.J. (1979). Mechanism of fluid and electrolyte secretion in the germ-free rat cecum. *Dig. Dis. Sci.* 24, 551–559.
  40. Wu, Y., Yang, S., Ma, J., Chen, Z., Song, G., Rao, D., Cheng, Y., Huang, S., Liu, Y., Jiang, S., et al. (2022). Spatiotemporal Immune Landscape of Colorectal Cancer Liver Metastasis at Single-Cell Level Spatial and Cellular Landscape of CRLM. *Cancer Discov.* 12, 134–153.
  41. Macpherson, A.J., and Harris, N.L. (2004). Interactions between commensal intestinal bacteria and the immune system. *Nat. Rev. Immunol.* 4, 478–485.
  42. Chhabra, P., Spano, A.J., Bowers, D., Ren, T., Moore, D.J., Timko, M.P., Wu, M., and Brayman, K.L. (2018). Evidence for the Role of the Cecal Microbiome in Maintenance of Immune Regulation and Homeostasis. *Ann. Surg.* 268, 541–549. <https://doi.org/10.1097/SLA.0000000000002930>.
  43. Barber, E.K., Dasgupta, J.D., Schlossman, S.F., Trevillyan, J.M., and Rudd, C.E. (1989). The CD4 and CD8 antigens are coupled to a protein-tyrosine kinase (p56lck) that phosphorylates the CD3 complex. *Proc. Natl. Acad. Sci. USA* 86, 3277–3281.
  44. Brand, S., Dambacher, J., Beigel, F., Zitzmann, K., Heeg, M.H.J., Weiss, T.S., Prüfer, T., Olszak, T., Steib, C.J., Storr, M., et al. (2007). IL-22-mediated liver cell regeneration is abrogated by SOCS-1/3 overexpression *in vitro*. *Am. J. Physiol. Gastrointest. Liver Physiol.* 292, G1019–G1028.
  45. Sullivan, Z.A., Khoury-Hanold, W., Lim, J., Smillie, C., Biton, M., Reis, B.S., Zwick, R.K., Pope, S.D., Israni-Winger, K., Parsa, R., et al. (2021).  $\gamma\delta$  T cells regulate the intestinal response to nutrient sensing. *Science* 371, eaba8310.
  46. Talbot, J., Hahn, P., Kroehling, L., Nguyen, H., Li, D., and Littman, D.R. (2020). Feeding-dependent VIP neuron-ILC3 circuit regulates the intestinal barrier. *Nature* 579, 575–580.
  47. Björntorp, P., and Rosmond, R. (2000). Obesity and cortisol. *Nutrition* 16, 924–936.
  48. Herbert, J. (2013). Cortisol and depression: three questions for psychiatry. *Psychol. Med.* 43, 449–469.
  49. Platten, M., Nollen, E.A.A., Röhrig, U.F., Fallarino, F., and Opitz, C.A. (2019). Tryptophan metabolism as a common neurodegenerative target in cancer, neurodegeneration and beyond. *Nat. Rev. Drug Discov.* 18, 379–401.
  50. Schwarcz, R., and Stone, T.W. (2017). The kynurenine pathway and the brain: Challenges, controversies and promises. *Neuropharmacology* 112, 237–247.
  51. Cai, M., Zhang, W., Weng, Z., Stetler, R.A., Jiang, X., Shi, Y., Gao, Y., and Chen, J.J.A. (2017). Promoting neurovascular recovery in aged mice after ischemic stroke-prophylactic effect of omega-3 polyunsaturated fatty acids. *Aging Dis.* 8, 531–545.
  52. Carta, G., Murru, E., Banni, S., and Manca, C. (2017). Palmitic acid: physiological role, metabolism and nutritional implications. *Front. Physiol.* 8, 902.
  53. Chilton, F.H., Rudel, L.L., Parks, J.S., Arm, J.P., and Seeds, M.C. (2008). Mechanisms by which botanical lipids affect inflammatory disorders. *Am. J. Clin. Nutr.* 87, 498S–503S.
  54. Swanson, D., Block, R., and Mousa, S.A. (2012). Omega-3 fatty acids EPA and DHA: health benefits throughout life. *Adv. Nutr.* 3, 1–7.
  55. Dyerberg, J., Bang, H.O., Stoffersen, E., Moncada, S., and Vane, J.R. (1978). Eicosapentaenoic acid and prevention of thrombosis and atherosclerosis? *Lancet* 2, 117–119. [https://doi.org/10.1016/s0140-6736\(78\)91505-2](https://doi.org/10.1016/s0140-6736(78)91505-2).
  56. Korotkova, M., and Lundberg, I.E. (2014). The skeletal muscle arachidonic acid cascade in health and inflammatory disease. *Nat. Rev. Rheumatol.* 10, 295–303. <https://doi.org/10.1038/nrrheum.2014.2>.
  57. Vincent, A.D., Wang, X.-Y., Parsons, S.P., Khan, W.I., and Huizinga, J.D. (2018). Abnormal absorptive colonic motor activity in germ-free mice is rectified by butyrate, an effect possibly mediated by mucosal serotonin. *Am. J. Physiol. Gastrointest. Liver Physiol.* 315, G896–G907.
  58. Lomasney, K.W., Houston, A., Shanahan, F., Dinan, T.G., Cryan, J.F., and Hyland, N.P. (2014). Selective influence of host microbiota on cAMP-mediated ion transport in mouse colon. *Neuro Gastroenterol. Motil.* 26, 887–890.
  59. Abrams, G.D., Bauer, H., and Sprinz, H. (1962). Influence of the Normal Flora on Mucosal Morphology and Cellular Renewal in the Ileum. A Comparison of Germ-free and Conventional Mice (MOUNT SINAI HOSPITAL NEW YORK).
  60. Kennedy, E.A., King, K.Y., and Baldrige, M.T. (2018). Mouse microbiota models: comparing germ-free mice and antibiotics treatment as tools for modifying gut bacteria. *Front. Physiol.* 9, 1534.
  61. Calamita, G., Mazzone, A., Cho, Y.S., Valenti, G., and Svelto, M. (2001). Expression and localization of the aquaporin-8 water channel in rat testis. *Biol. Reprod.* 64, 1660–1666.
  62. Shao, H., Pan, S., Lan, Y., Chen, X., Dai, D., Peng, L., and Hua, Y. (2022). Tanshinone IIA increased amniotic fluid volume through down-regulating placental AQP8 expression via inhibiting the activity of GSK-3 $\beta$ . *Cell Tissue Res.* 389, 547–558.
  63. Hua, Y., Ding, S., Cheng, H., Luo, H., and Zhu, X. (2017). Tanshinone IIA increases aquaporins expression in human amniotic epithelial WISH cells by stimulating GSK-3 $\beta$  phosphorylation. *Clin. Chim. Acta* 473, 204–212.
  64. Almasalmeh, A., Krenc, D., Wu, B., and Beitz, E. (2014). Structural Determinants of the Hydrogen Peroxide Permeability of Aquaporins (Wiley Online Library).
  65. Gury-BenAri, M., Thaïs, C.A., Serafini, N., Winter, D.R., Giladi, A., Lara-Astiaso, D., Levy, M., Salame, T.M., Weiner, A., David, E., et al. (2016). The spectrum and regulatory landscape of intestinal innate lymphoid cells are shaped by the microbiome. *Cell* 166, 1231–1246.e13.
  66. Clavel, T., Gomes-Neto, J.C., Lagkouvardos, I., and Ramer-Tait, A.E. (2017). Deciphering interactions between the gut microbiota and the immune system via microbial cultivation and minimal microbiomes. *Immunol. Rev.* 279, 8–22.
  67. Michaudel, C., and Sokol, H. (2020). The gut microbiota at the service of immunometabolism. *Cell Metab.* 32, 514–523.
  68. Schluter, J., Peled, J.U., Taylor, B.P., Markey, K.A., Smith, M., Taur, Y., Niehus, R., Staffas, A., Dai, A., Fontana, E., et al. (2020). The gut microbiota is associated with immune cell dynamics in humans. *Nature* 588, 303–307.
  69. Tsang, D.K.L., Wang, R.J., De Sa, O., Ayyaz, A., Foerster, E.G., Bayer, G., Goyal, S., Trcka, D., Ghoshal, B., Wrana, J.L., et al. (2022). A single cell survey of the microbial impacts on the mouse small intestinal epithelium. *Gut Microb.* 14, 2108281.
  70. Wen, B., Mei, Z., Zeng, C., and Liu, S. (2017). metaX: a flexible and comprehensive software for processing metabolomics data. *BMC Bioinf.* 18, 183. <https://doi.org/10.1186/s12859-017-1579-y>.
  71. DeTomaso, D., Jones, M.G., Subramaniam, M., Ashuach, T., Ye, C.J., and Yosef, N. (2019). Functional interpretation of single cell similarity maps. *Nat. Commun.* 10, 4376.
  72. Dobin, A., Davis, C.A., Schlesinger, F., Drenkow, J., Zaleski, C., Jha, S., Batut, P., Chaisson, M., and Gingeras, T.R. (2013). STAR: ultrafast universal RNA-seq aligner. *Bioinformatics* 29, 15–21. <https://doi.org/10.1093/bioinformatics/bts635>.
  73. Biancalani, T., Scalia, G., Buffoni, L., Avasthi, R., Lu, Z., Sanger, A., Tokcan, N., Vanderburg, C.R., Segerstolpe, A., Zhang, M., et al. (2021). Deep learning and alignment of spatially resolved single-cell transcriptomes with Tangram. *Nat. Methods* 18, 1352–1362. <https://doi.org/10.1038/s41592-021-01264-7>.
  74. Pedregosa, F., Varoquaux, G., Gramfort, A., Michel, V., Thirion, B., Grisel, O., Blondel, M., Prettenhofer, P., Weiss, R., and Dubourg, V. (2011). Scikit-learn: Machine learning in Python. *J. Mach. Learn. Res.* 12, 2825–2830.

## STAR★METHODS

### KEY RESOURCES TABLE

REAGENT or RESOURCE	SOURCE	IDENTIFIER
<b>Antibodies</b>		
Rabbit Anti-Aquaporin 8 antibody	Bioss antibodies	bs-6786R
<b>Critical commercial assays</b>		
DNBelab C-Series Single Cell Library Preparation Kit	MGI	1000021082
Chromium Next GEM Single cell 3' kit v3.1	10x Genomics	PN-1000269
All original code	This paper	<a href="https://github.com/1014723815/GF_SPF_cecum.git">https://github.com/1014723815/GF_SPF_cecum.git</a>
<b>Deposited data</b>		
Raw and processed scRNA-seq data	This paper	CNP0004192
Raw and processed ST data	This paper	CNP0004192
<b>Software and algorithms</b>		
Cell Ranger	10x Genomics	Version 6.0.2
Seurat	<a href="https://satijalab.org/seurat/index.html">https://satijalab.org/seurat/index.html</a>	Version 4.0.3
MAST	<a href="https://www.bioconductor.org/packages/release/bioc/html/MAST.html">https://www.bioconductor.org/packages/release/bioc/html/MAST.html</a>	Version 1.20.0
CellChat	<a href="https://www.bioconductor.org/packages/release/bioc/html/MAST.html">https://www.bioconductor.org/packages/release/bioc/html/MAST.html</a>	Version 1.1.3
scMetabolism	<a href="https://github.com/wu-yc/scMetabolism/tree/main">https://github.com/wu-yc/scMetabolism/tree/main</a>	Version 0.2.1
Fastp	<a href="https://github.com/OpenGene/fastp">https://github.com/OpenGene/fastp</a>	Version 0.23.1
BayesSpace	<a href="https://edward130603.github.io/BayesSpace/articles/BayesSpace.html">https://edward130603.github.io/BayesSpace/articles/BayesSpace.html</a>	Version 1.4.1
Tangram	<a href="https://github.com/tangrams/tangram">https://github.com/tangrams/tangram</a>	Version 1.0.3
clusterProfiler	<a href="https://bioconductor.org/packages/release/bioc/html/clusterProfiler.html">https://bioconductor.org/packages/release/bioc/html/clusterProfiler.html</a>	Version 4.2.2
<b>Other</b>		
DNBSEQ-T7 sequencing platform	MGI	900-000129-00

### RESOURCE AVAILABILITY

#### Lead contact

Additional information and requests for resources and reagents should be directed to and will be completed by the lead contact, Xiaodong Fang ([fangxd@bgi.com](mailto:fangxd@bgi.com)).

#### Materials availability

This study did not generate any unique reagents.

#### Data and code availability

- The data that support the findings of this study have been deposited at CNGB Sequence Archive (CNSA) of China National GeneBank DataBase (CNGBdb) (<https://db.cngb.org/cnsa/>) and are publicly available as of the date of publication. Accession numbers are listed in the [key resources table](#).
- All original code has been deposited at Github and is publicly available as of the date of publication. DOIs are listed in the [key resources table](#).
- Any additional information required to reanalyze the data reported in this paper is available from the [lead contact](#) upon request.

## EXPERIMENTAL MODELS AND STUDY PARTICIPANT DETAILS

### Mouse rearing

GF and SPF mice were both of the KM(Kunming) mouse strain and were sourced from the Experimental Animal Center of Huazhong Agricultural University (Wuhan, China). Both GF and SPF mice ate GF mouse chow. The difference is that the chow for GF mice is sterilized to completely kill microorganisms. The chow for SPF mice is not sterilized. In addition, GF mice were reared in specific sterile incubators to ensure a completely sterile environment. 13 GF mice and 13 SPF mice were reared to adulthood. Using male 10-week-old mice. All mice were executed by cervical dislocation. No blinding of samples was performed.

### Ethics approval

This study did not involve human participants. The animal protocol was approved by BGI (BGI-IRB A21028).

## METHOD DETAILS

### Single cell transcriptome sample processing and sequencing

Two GF and two SPF mice were randomly selected to collect the cecum and colon for single cell transcriptome sequencing. The residual contents of the cecum were removed in pre-cooled PBS solution. The washed cecum and colon tissue was cut into small pieces the size of green beans and preserved in pre-cooled fresh sample preservation solution for sample processing within 24 hours. Cell separation was performed on the collected samples. Selection of colon and cecum from 1 GF mouse and 1 SPF mouse for library construction using DNBelab C-Series Single Cell Library Preparation Kit (MGI, 1000021082). The identified libraries were sequenced at the DNBSEQ-T7 sequencing platform (BGI, Shenzhen, China). Single cell RNA sequencing was performed on cecum samples from the remaining 1 GF mouse and 1 SPF mouse using Chromium Next GEM Single cell 3' kit v3.1 (10x Genomics), followed by library construction according to the manufacturer's recommendations and sequencing on the MGISEQ-2000 platform (BGI, Shenzhen, China). No sequenced samples were excluded from the analysis.

### Spatial transcriptome sample processing and sequencing

One GF mouse and one SPF mouse were randomly selected and the cecum and colon were taken. Removal of residual intestinal contents by washing in pre-cooled PBS solution, removed and dried on dust-free paper. Then, sections are selected at the appropriate location and affixed to a Stereo-seq Spatial Transcriptome SC (Stereo Chip) chip, and sections are fixed in pre-cooled methanol solution. The sections were stained with tissue fluorescent staining solution (ssDNA) and photographed. Permeabilization was carried out at 37°C for 6 min. Reverse transcription was carried out at 42°C for 1 h. After tissue removal, cDNA release was carried out at 55°C for 3 h. The released cDNA was recovered and PCR amplification was carried out under standard systems. Magnetic beads were recovered from the amplified samples to obtain a final qualified pre-banking cDNA solution. The pre-built cDNA samples were cyclized, interrupted, recovered and concentration measured to finally obtain qualified library samples. Libraries were sequenced by DNBSEQ-T7 sequencing platform (BGI, Shenzhen, China).

### Sample preparation and data analysis for non-targeted metabolome

Ten GF mice and ten SPF mice were obtained. The mice were executed and the contents of the cecum were collected. The samples were snap frozen in liquid nitrogen and processed within 48h. Non-targeted metabolomic analysis was performed by LC-MS/MS technique using a high resolution mass spectrometer Q Exactive HF (Thermo Fisher Scientific, USA), with data collected in both positive and negative ion mode to improve metabolite coverage. LC-MS/MS data processing was performed using Compound Discoverer 3.1 (Thermo Fisher Scientific, USA) software, mainly for peak extraction, peak alignment and compound identification. Data pre-processing, statistical analysis and metabolite classification annotation and functional annotation were performed using metaX as well as the Metabolome Information Analysis process.<sup>70</sup> The raw multivariate data were downscaled by PCA (Principal Component Analysis) to analyze the grouping, trends (similarities and differences within and between sample groups) and outliers (presence of outlier samples) of the observed variables in the dataset. The KEGG and BGI databases were used for metabolite detection. The VIP values of the first two principal components of the PLS-DA (Partial Least Squares Method-Discriminant Analysis) model were used, combined with the Fold change and Student's t test obtained from the univariate analysis. The results of the univariate analysis were used to screen for differential metabolites. Our differential metabolite screening criteria were 1)  $VIP \geq 1$  for the first two principal components of the PLS-DA model, 2)  $Fold-Change \geq 1.2$  or  $\leq 0.83$ , and 3)  $q\text{-value} < 0.05$ .

## QUANTIFICATION AND STATISTICAL ANALYSIS

### Single cell data pre-processing

To process raw RNA-seq data, we employed Cell Ranger (v6.0.2), which was used to aggregate unique molecular identifiers and map them to the mm10/GRCm38 transcriptome. The resultant expression matrices were analyzed via Seurat (4.0.3) (<http://satijalab.org/seurat/>). To integrate the datasets, we used the "FindIntegrationAnchors" and "IntegrateData" functions in Seurat to integrate data from the C4 platform and the 10X genomics platform. To remove low-quality data, we filtered out cells with fewer than 200 genes, genes expressed in fewer than 3 cells, and excluded more than 50% of mitochondrial genes. We identified principal components using the first 2000 variable features and down-scaled and clustered the data using the "RunPCA" and "RunUMAP" functions in Seurat. The single cell transcriptome from [Figure S2A](#)

represents the original cluster annotation results at 0.5 resolution. Merging the same subclasses of [Figure S2A](#) to form the broad class results of [Figure 2A](#). Finally, cell cluster identities were annotated manually using known marker genes from published articles,<sup>24–28</sup> with guidance from the Mouse Cell Atlas (<https://bis.zju.edu.cn/MCA/index.html>) database.

### Analysis of cellular interactions

In order to explore the strength and variability of inter-cellular interactions in the cecum. We used CellChat (v1.1.3) to assess cell-cell interactions in different samples (GF and SPF mice) and how signaling pathways interact across cellular identities.<sup>35</sup> We followed the official cell-chat process to merge GF and SPF datasets, create “cellchat” objects and use the “CellChatDB.mouse” database for subsequent analysis.

### Analysis of cellular metabolic activity

In order to assess changes in the metabolic intensity of epithelial cells in GF&SPF mice. We used scMetabolism (v0.2.1) to quantify metabolic activity at the single-cell level.<sup>40</sup> The method is based on a conventional single-cell matrix file and uses the VISION algorithm to score each cell.<sup>71</sup> The final activity score of the cell in each metabolic pathway was obtained. The results included 85 KEGG pathways and 82 REACTOME entries.

### Spatial data pre-processing

After obtaining spatial transcriptome sequencing data, we used “ST\_BarcodeMap” to extract read pairs with valid CIDs, converting the CID sequences of the reads into spatial location information for the reads. We then used Fastp (v0.23.1) to filter low quality reads to obtain clean reads. Clean reads were aligned to the mouse reference genome (GRCm39) using STAR and the number of reads aligned to regions such as exons, introns and intergenic regions was calculated from the gene annotation file.<sup>72</sup> Correspondence between uniquely mapped reads aligned to the reference genome and genes was calculated using Bam2Gem and expression levels of all genes were calculated based on MID correction. By quantifying gene expression, the final output is an expression matrix of all genes detected on the tissue section, which is stored in a GEM format file. Bin1 denotes a point in the section with a diameter of 220 nm and BinN denotes the combined Bin in an  $N \times N$  squared region. we selected Bin20, Bin50 and cell-Bin data for subsequent analysis. The B50 data is used to show an overall landscape of the cecum section. The B20 data is used to show the detailed landscape. In addition, we segmented the cells based on the ssDNA picture and reconstructed the spatial expression data from the segmentation results to generate cell-Bin data, where a point represents a cell. The cell-Bin data is used to display the detailed landscape.

### Spatial clustering

We used BayesSpace (v1.4.1) for spatial clustering of spatial transcriptome slices.<sup>30</sup> This method uses information from spatial neighbourhoods to enhance the resolution of spatial transcriptome data and perform clustering analysis.

### Deconvolution

We used the Cell2location method to deconvolve the spatial transcriptome microarray using single-cell transcriptome data as the reference dataset.<sup>36</sup> tangram (v1.0.3) was used to predict the cellular composition of each Bin50.<sup>73</sup> We chose to use the p-value as a criterion to select the five most important marker genes for each cell type as signals. “map\_cells\_to\_space” function was used to obtain a mapping of single cell data to spatial data. Finally, the signal intensity of each cell under each merged box was obtained by the “project\_cell\_annotations” function. The “visualization” of the various cell compositions was implemented by the “plot\_space” function of Cell2location and the NMF algorithm was implemented by the NMF module in “sklearn.decomposition”.<sup>74</sup>

### Statistics and reproducibility

All cecum spatial transcriptomics data shown in the main and supplementary panels were generated from GF n=1 and SPF n=1 for a total of two mice. Cecum single-cell transcriptomics data were generated from GF n=2 and SPF n=2 for a total of four mice. Cecum metabolomics data were generated from GF n=10 and SPF n=10 for a total of 20 mice. Cecum anatomical data were generated from GF n=13 and SPF n=13 for a total of 26 mice. Spatial data for the colon were generated from GF n=1 and SPF n=1 for a total of two mice. Single cell data for the colon were generated from GF n=1 and SPF n=1 for a total of two mice. Statistical analysis of anatomical data from [Figures 1D](#) and [1E](#) and statistical analysis of metabolites from [Figure 6C](#) were performed using Student’s t-test two-tailed test. The statistical analysis of epithelial cell proportions from [Figure 4C](#) was performed using Fisher’s exact test two-tailed test. Gene expression statistics from [Figures 4G](#), [7F](#), [S7C](#), and [S7D](#) were analyzed using Wilcoxon test two-tailed test.

### Immunofluorescence

8  $\mu$ m thick sections of cecum were cut and fixed in cold methanol for 20 minutes. After three washes with PBS, the tissue sections were enclosed in containment buffer (3% BSA, 0.3% Triton™ X-100 in PBS) for 30 min and then overnight at 4°C. The next day, the sections were washed with PBS and incubated with a fluorescent-conjugated secondary antibody for 1 h. The sections were fixed in cold methanol for 20 min. The next day, the tissue sections were washed with PBS and incubated with fluorescence-conjugated secondary antibodies for 1

h. Fixed medium containing DAPI was used to visualize the nuclei and preserve the slides. Antibodies used were as follows: polyclonal antibody to AQP8 (bs-6786R).

#### **Total osmolality determination**

The contents of the cecum of adult GF mice (n=3) and SPF mice (n=3) were taken. The contents were centrifuged at 10,000 g for 15 min and the supernatant was taken. The total osmotic pressure of the supernatant was determined by referring to Chinese Pharmacopoeia 2020 Edition Part Four General Rule 0632 Osmotic Pressure Molar Concentration Determination Method.